People's Democratic Republic of Algeria
Ministry of Higher Education and Scientific Research

University M'Hamed BOUGARA – Boumerdes

Institute of Electrical and Electronic Engineering

Department of Power and Control Engineering

Final Year Project Report Presented in Partial Fulfilment of
the Requirements for the Degree of

MASTER

In **Power Engineering**

Option: **Power Engineering**

Title:

Enhanced Direct Torque Control of Permanent Magnet Synchronous Motor Using Sliding Mode Control Theory

Presented by:

- **Raid Bencheikh**

Supervisor:

- **Abdelkarim Ammar**

Acknowledgement

First and foremost, Alhamdulillah I would like to praise and thank God, the almighty, who has granted countless blessing, knowledge, and opportunity to me, so that I have been finally able to accomplish the thesis.

The completion of this study would have been not possible if not dependent on the steadfast support and encouragement of my beloved mother **(zemouli Samia)** and my father **(Bencheikh Belkacem)**. They hence paid equal contribution to the study for which I always feel profound gratitude in my heart.

I would like to express here the very thanks to my dissertation advisor, **Prof. Dr. Abdelkarim Ammar** for his precious and continuous guidance and support throughout the course of this study. His dedicated supervision and constant encouragement towards the completion of this thesis encouraged me to do my best. His wide knowledge and his logical way of thinking have been of great value for me.

I would also like to express my sincere appreciation to **Mr. Zakaria Rabiai** and **Mr. Youcef Grainat** for their support and encouragement in the completion of this thesis. Their willingness to give guidance and supervision becomes a great help to me.

I owe my loving thanks to my brother **Noufel** and my sisters **wissal** and **rinad** and not to forget my dearest **grandmother** and my **auntie** Without their encouragement and understanding, it would have been impossible for me to finish this work.

My special gratitude goes to my dear friends **Bencheikh Abdeljabbar** and **Djemaoui Mahmoud** for being very supportive in spiritual, their optimistic attitudes especially encouraged me not to give up even facing any obstacles or difficulties.

Abstract

Enhanced Direct Torque Control of Permanent Magnet Synchronous Motor Using Sliding Mode Control Theory

The direct torque control (DTC) was proposed as an alternative to the vector control in the middle of 1980s for AC machines control. This strategy is based on the direct determination of inverter switching states and offers a simpler scheme and less sensitivity to machine parameters. However, the variable switching frequency of DTC causes high flux and torque ripples which lead to an acoustical noise and degrade the performance of the control technique, especially at low-speed regions.

In the objective of improving the performance of DTC for the Permanent magnet synchronous machine, this thesis addresses the most important points concerning this issue. The reduction of high ripples, which are the major drawbacks, by applying a constant switching frequency using the space vector modulation (SVM). Then, this thesis presents the sliding mode control to improve the speed control in DTC algorithm and to ensure a robust control against different uncertainties and external disturbances.

Keyword: Permanent Magnet Synchronous Machine (PMSM), Direct Torque Control (DTC), Space Vector Modulation (SVM), Sliding Mode Control (SMC), MATLAB/Simulink.

List of Figures

List of tables

List of Abbreviations

PMSM	Permanent Magnet Synchronous Machine
VSI	Voltage Source Inverter
DTC	Direct Torque Control
SVM	Space Vector Modulation
VC	Vector Control
FOC	Field Oriented Control
DSC	Direct Self Control
THD	Total Harmonic Distortion
DQ axis	Direct and Quadrature axis
DSP	Digital Signal Processor
AC	Alternative Current.
DC	Direct Current.
DFOC	Direct-Field Oriented Control.
PWM	Pulse Width Modulation.
SFOC	Stator Filed Oriented Control.
VFD	Variable Frequency Drives.
VSC	Variable Structure Control.

Contents

General Introduction

Nowadays, the AC machines have replaced the DC machines in industry applications because of their advantages, such as, the reliability and the lack of commutator and brushes which make them able to work under unfriendly conditions. The most popular AC machines are the induction motors (IMs) and the permanent magnet synchronous motors (PMSMs). They are used in various industrial applications, electric vehicles (EV), tools and drives etc.

Recently, an increased interest in application of permanent magnet synchronous motors (PMSM) in speed-controlled drives has been observed. This is stimulated mainly by:

- Development of modern high switching frequency semiconductor power devices (as for example IGBT modules of 5-th generation),
- New rare earth magnetic materials as samarium-cobalt (Sm-Co) or neodymium-iron boron (Nd-Fe-B).
- Specialized digital signal processor (DSP) for AC drive applications with integrated PWM function, A/D converters as well as processing of encoder signals (e.g. ADMC401, TMS320FL24XX, TMS320FL28XX).

Synchronous motors with an electrically excited rotor winding have a conventional three phase stator winding (called armature) and an electrically excited field winding on the rotor, which carries a DC current. The armature winding is similar to the stator of induction motor. The electrically excited field winding can be replaced by permanent magnet (PM). The use of permanent magnets has many advantages including the elimination of brushes, slip rings, and rotor copper losses in the field winding. It leads to higher efficiency. Additionally, since the copper and iron losses are concentrated in the stator, cooling of machines through the stator is more effective. The lack of field winding and higher efficiency results in reduction of the machine frame size and higher power/weight ratio.

In the early decades, the PMSMs have been operated directly from the grid Under a fixed frequency/speed. Later, with the development of modern semiconductor devices and power electronic converters, these machines had become able to operate with adjustable frequency/speed by supplying them through a power converter like the voltage source inverter (VSI). The employment of the variable speed motor drive

in open loop may offer a satisfied performance at steady state without need of speed regulation for simple applications. But, in cases where the drive requires fast dynamic response and accurate speed, the open loop control becomes unsatisfactory. Therefore, it is necessary to operate the motor in a closed loop mode. Several techniques have been proposed for this purpose. They are classified mainly into scalar and vector controls. The scalar control, that called also volts/hertz, is a simple strategy which is applied to control the speed of PMSMs based on the constant ratio of voltage magnitude and frequency using the steady-state equivalent circuit model of the machine. However, this method does not dedicate for high performance applications due to its slow response and the existence of coupling between torque and flux. The vector control, which is known also by the field-oriented control (FOC), was developed to overcome the limitation of the scalar control. It was presented in the 1970s by Hasse and Blaschke [6] to provide an independent control of torque and flux in similar way to the separate excitation DC machine. The vector representation of the motor quantities makes it valid to work in both steady and dynamic conditions; this achieves a good transient response. In the control algorithm of FOC based on the transformation to the synchronous frame, all quantities will appear as DC quantities. Nevertheless, the main disadvantages of FOC are the coordinates transformation which needs the flux angle that cannot be directly measured, in addition, the sensitivity to the variation of the machine parameters, like the stator and the rotor resistances.

Another method guarantees a separated flux and torque control is called Direct Torque Control (DTC). It was introduced by Takahashi and Nagochi in the middle of 1980s in Japan [7] In contrast to FOC, this control is completely done in stationary frame (stator fixed coordinates). Furthermore, DTC generates the inverter gating signals directly through a look up switching table and the use of modulator is not necessary. It offers an excellent torque response using less model's parameters than FOC. Due to its simplicity and very fast response it can be so applicable for high performance drive applications [43]. However, the standard DTC method suffers from high flux and torque ripples owing to the use of hysteresis controllers. The insertion of the space vector modulation (SVM) was a very useful solution [44]. This method, known by SVM-DTC, reduces the high ripples level in spite of its complexity.

The linear proportional integral differential (PID) controllers have encountered a wide interest in the industrial applications. However, extra extensions should be

made to fulfill an acceptable behavior like the output limitation and anti-windup. Nevertheless, another important issue is proposed for stability reasons in the control loop. It may be affected by the variation in parameters due to environment conditions and the external disturbance during operating. Consequently, the use of linear methods cannot achieve high promising performance.

The development of robust control methods to solve this problem has made a big achievement recently. The nonlinear controllers can offer several advantages compared to linear control schemes. Among the interest researches in the field of nonlinear control techniques is the sliding mode control (SMC) [47; 28].

The sliding mode control is featured by high robust behavior while the presence of uncertainties. SMC forces the system trajectory to slide along the switching surface by determined control law. The most powerful advantages of the SMC are the high robustness against the different system uncertainties, the rapid dynamic response and the simple implementation.

The objective of this thesis is the improvement of the performance of DTC driven PMSM using space vector modulation and sliding mode control.

Organization of the thesis

The first chapter summarizes a background about the permanent magnet synchronous machine, its design and application. Then it presents the dynamic modeling of PMSM.

The second chapter presents a comparative study between the classical and the constant switching frequency DTC methods. The third chapter presents the sliding mode control in order to improve the speed regulation loop of DTC-SVM.

Finally, chapter four present the simulation and the comparison of different presented control strategies for the PMSM.

1.1. Overview

Electric motors have been commonly used in many applications such as household appliances, hybrid and electric vehicles, off road traction systems and industrial processes as a means to convert electrical energy into mechanical energy. Being the largest consumer of electric power, electric motors have always received the attention of researchers.

Among the different types of electric motors, permanent magnet synchronous motors (PMSM) which do not require brushes for commutation, are gaining attention due to their high performance and efficient operation. Having permanent magnets on the rotor eliminates the rotor current requirement to generate the rotor field. Elimination of the rotor current enables more efficient operation compared to similar sized induction motors.

Brushless operation ensures lower maintenance requirements and also eliminates the losses in the brushes. Properties such as lower maintenance cost, high torque density, and low torque to inertia ratio are making PMSMs attractive alternatives over other motors in applications such as spindle drives, air-conditioning compressors, cooling towers, electric vehicles and integrated starters and alternators.

1.2. Classification of Permanent Magnet Synchronous Motors

The physical characteristics of the PMSM are associated with its rotor and stator structures. The **Stator** is composed of a three-phase wound such that the Electromotive Forces (EMF) are generated by the rotation of the rotor field. Furthermore, the EMF can be sinusoidal or trapezoidal. This wound is represented by the three axes (a, b, c) phase shifted, one from the other, by 120 electrical degrees [1].

The **Rotor** incorporates permanent magnets to produce a magnetic field. Regarding winding, the permanent magnets have the advantage to eliminate the brushes, the rotor losses, and the need for a controlled DC source to provide the excitation current. However, the amplitude of the rotor flux is constant. On the other hand, there exist several ways to place the magnets in the rotor as shown in **Fig. 1.1**

Following the magnet position, the PMSM can be classified into four major types:

1.2.1 Surface mounted magnets type

The magnets are placed on the surface of the rotor using high strength glue. They present a homogeneous gap. The motor is a non-salient pole and the inductances do not depend on the rotor position (**Fig. 1.1a**). The inductance of the axe-*d* is equal to those of the axe-*q*. This configuration of the rotor is simple to obtain. This type of rotor is the most usual. On the other

hand, the magnets are exposed to a demagnetizing field. Moreover, they are subject to the centrifuge forces which can cause the detachment of the rotor.

1.2.2 Inset magnets type

The inset magnets are placed on the surface of the rotor. However, the space between the magnets is filled with iron (**Fig. 1.1b**). Alternation between the iron and the magnets causes a salient effect. The inductance in the *d*-axe is slightly different from the inductance in the *q*-axe.

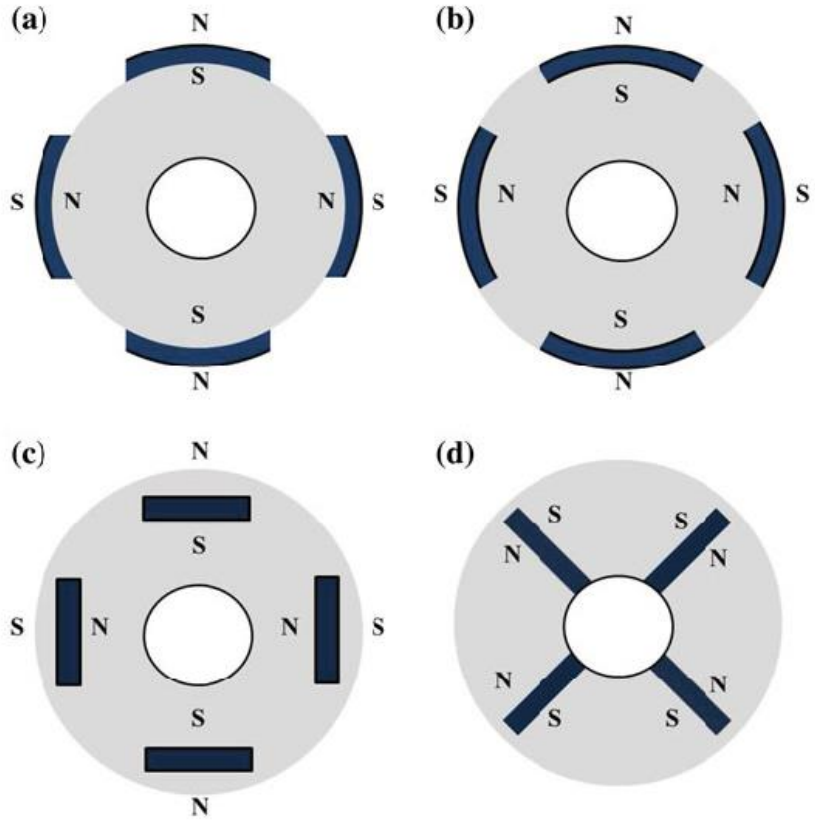

Fig. 1.1: PMSM rotor permanent magnets layout: **a** surface permanent magnet, **b** inset permanent magnets, **c** interior permanent magnets, **d** flux concentrating.

1.2.3. Interior magnets type

The magnets are integrated in the rotor's body (**Fig. 1.1c**): the motor is a salient pole type. In this case, the rotor magnetism is anisotropic, the inductances depend on the rotor position. The magnets are placed in the rotor, providing more mechanical durability and robustness at high speeds. On the other hand, this motor is more expensive to manufacture and more complex to control.

1.2.4. Flux concentrating type

As shown in **Fig. 1.1d**, the magnets are deeply placed in the rotor's body. The magnets and their axes are radial. The flux on a polar arc of the rotor is a result of two separated magnets.

The advantage of this configuration is the possibility to concentrate the flux generated by the permanent magnets in the rotor and to obtain a stronger induction in the gap. This type of machine has a salience effect. However, surface permanent magnet synchronous motors and interior permanent magnet synchronous motors are the most used in the industry.

Furthermore, the permanent magnet synchronous motors can be classified according to the electromotive force profiles as shown in the following diagram [2] :

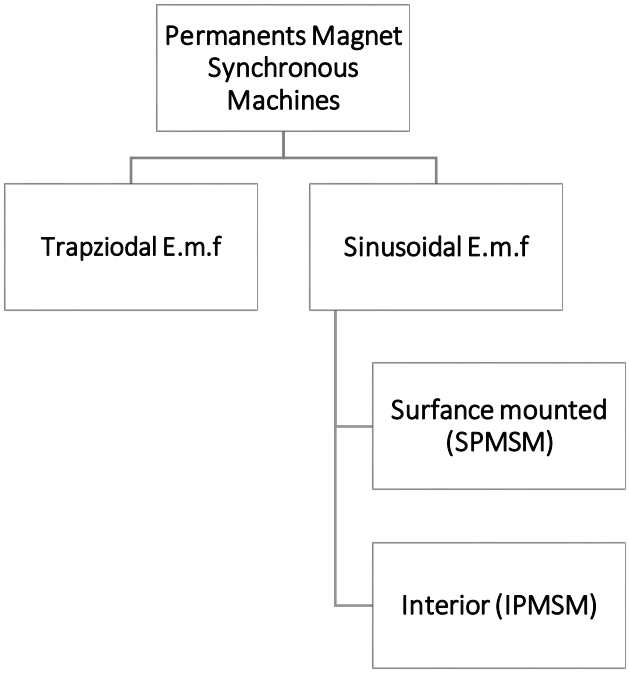

Fig.1.2: General classification permanents magnet synchronous machines.

Particularly, the synchronous machines with sinusoidal EMF are classified into two subcategories in terms of magnets position

1. **Non-salient Poles**: the magnets are located in the rotor surface (**Fig. 1.1a**): Surface Permanent Magnet Synchronous Motor (SPMSM)

2. Salient Poles: the magnets are buried into the rotor (**Fig. 1.1c, d**): Interior Permanent Magnet Synchronous Motor (IPMSM).

1.3. Applications, advantages and disadvantages of PMSM

The requirement of variable speed drives with respect to single speed drives are necessary. Variable speed drives changed the field of motor which is used in such drives till the last decade, the induction motor and Direct Current motor have dominated as mechanical energy conversion devices but now they are being replaced by BLDCs and PMSMs in the category of power application which ranges between 0-5kW. The applications of PMSM motors

between 0-5 kW are Robotics and factory automation (servo drives), printers/plotters, tape drivers, washers, blowers, compressors, Power steering, ventilation and air conditioning.

- **Advantages of PMSM**

PMSM have the following advantages over DC motors:

- Higher power density and smaller size.
- Sparkless operation (used in hazardous environment).
- Higher speed and Less noise.

Moreover, PMSM have the following advantages over induction motors:

Higher efficiency, Better heat transfer, Higher power density, resulting in smaller size, Higher power factor.

On the other hand, PMSM has the following disadvantages:

- Complex control, Demagnetization of the rotor magnet due to ageing.
- Reduction of torque production due to demagnetization of rotor magnet.
- Maintenance is often required for rotor magnet.

The above discussion justifies the choice made in the present research towards the need for research on PMSM.

- **Applications of PMSM:**

The good characteristics of the PMSM has ensured many applications, which include electric vehicles **Fig.1.3**, machine tool spindles, starter/generator units, robotics, aerospace actuators, electric wheelchairs, fan-type applications and turbo compressors and wind energy conversion system (WECS) **Fig.1.4.**

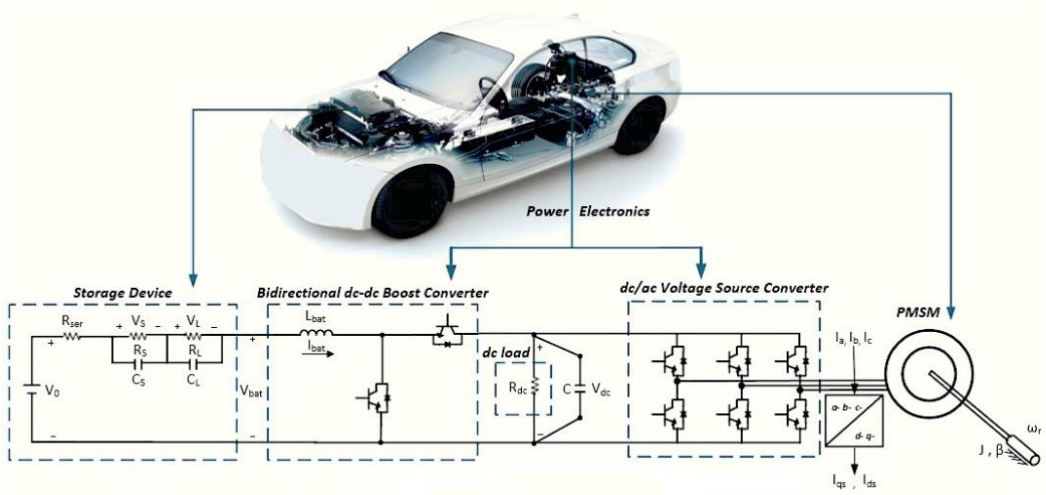

Fig.1.3: Block diagram of a Hybrid Electric Vehicle using PMSM drive.

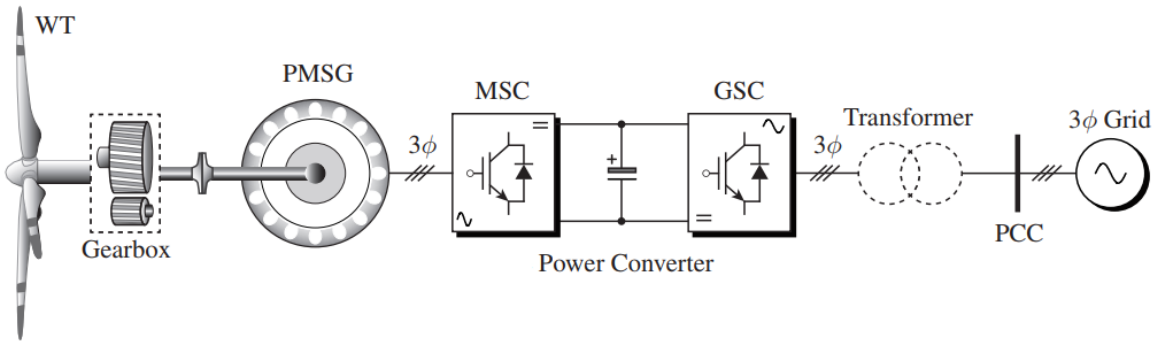

Fig.1.4: **WECS Block Diagram.**

1.4. Modeling of PMSM

The study of an electric motor behavior is a hard task and requires, first of all, good knowledge of its model to properly predict its dynamic behavior under different operating conditions. The study of an electric motor behavior is a hard task and requires, first of all, good knowledge of its model to properly predict its dynamic behavior under different operating conditions.

Modeling a permanent magnet synchronous motor is similar to a classical synchronous machine, except that the flux from the magnets is constant. Then, the model is derived from the classical synchronous machine [3].

1.4.1 Assumptions

To simplify the modeling of the machine, the following assumptions are introduced.

- The damping effect of the rotor is neglected.
- The magnetic circuit of the machine is not saturated.
- The distribution of the magnetomotive forces (MMF) is sinusoidal.
- The coupling capacitors between the windings are neglected.
- The hysteresis phenomena and the eddy currents are neglected.
- The gap irregularities owing to the stator slots are neglected.

Under these assumptions and using basic concepts, the electrical and mechanical equations describing the dynamical behavior of the PMSM are obtained.

1.4.2. Electric Equations

The three-phase stator voltage equations can be expressed as:

$$\begin{aligned} V_{sa} &= R_s I_{sa} + \frac{d\Psi_{sa}}{dt} \\ V_{sb} &= R_s I_{sb} + \frac{d\Psi_{sb}}{dt} \\ V_{sc} &= R_s I_{sc} + \frac{d\Psi_{sc}}{dt} \end{aligned} \quad \textbf{(1.1)}$$

Or in matrix form as :

$$[V_{sabc}] = R_s[I_{sabc}] + \frac{d[\Psi_{sabc}]}{dt} \quad (1.2)$$

Where

$[V_{sabc}] = [v_{sa}, v_{sb}, v_{sc}]^T$ are the voltages of each stator phase;

R_s is the stator resistance;

$[I_{sabc}] = [i_{sa}, i_{sb}, i_{sc}]^T$ are the phase stator currents.

$[\Psi_{sabc}] = [\Psi_{sa}, \Psi_{sb}, \Psi_{sc}]^T$ are the stator fluxes.

1.4.3. Magnetic Equations

The stator flux can be expressed as

$$[\Psi_{sabc}] = [L_{ss}][I_{sabc}] + [\Psi_{rabc}] \quad (1.3)$$

Where $[\Psi_{rabc}]$ is the rotor (permanent magnet) flux which is given as:

$$\begin{bmatrix} \Psi_{ra} \\ \Psi_{rb} \\ \Psi_{rc} \end{bmatrix} = \Psi_r \begin{bmatrix} \cos(p\theta_m) \\ \cos\left(p\theta_m - \frac{2\pi}{3}\right) \\ \cos\left(p\theta_m + \frac{2\pi}{3}\right) \end{bmatrix} \quad (1.4)$$

θ_m is the rotor position angle, and p as the pole pair number.

The inductance matrix $[L_{ss}]$ as:

$$[L_{ss}] = \begin{bmatrix} L_{aa} & M_{ab} & M_{ac} \\ M_{ba} & L_{bb} & M_{bc} \\ M_{ca} & M_{cb} & L_{cc} \end{bmatrix} \quad (1.5)$$

where:

L_{aa}, L_{bb}, L_{cc} are the self-inductances of the phases.

$M_{ab}, M_{ba}, M_{ac}, M_{ca}, M_{bc}, M_{cb}$ are the metual inductances between phases.

For the pole salient machines, the inductance matrix $[L_{ss}]$ can be expressed as:

$$[L_{ss}] = [L_{so}] + [L_{sv}] \quad (1.6)$$

Where:

$$[\mathrm{L}_{so}] = \begin{bmatrix} L_{so} & M_{so} & M_{so} \\ M_{so} & L_{so} & M_{so} \\ M_{so} & M_{so} & L_{so} \end{bmatrix}$$

and

$$[\mathrm{L}_{sv}] = L_{sv} \begin{bmatrix} \cos(2p\theta_m) & \cos(2p\theta_m) - \frac{2\pi}{3}) & \cos\left(2p\theta_m + \frac{2\pi}{3}\right) \\ \cos\left(2p\theta_m - \frac{2\pi}{3}\right) & \cos\left(2p\theta_m + \frac{2\pi}{3}\right) & \cos(2p\theta_m) \\ \cos\left(2p\theta_m + \frac{2\pi}{3}\right) & \cos(2p\theta_m) & \cos\left(2p\theta_m - \frac{2\pi}{3}\right) \end{bmatrix}$$

Then (1.2) become:

$$[\mathrm{V_{sabc}}] = \mathrm{R_s}[\mathrm{I_{sabc}}] + \frac{\mathrm{d}}{\mathrm{dt}}\{[\mathrm{L_{ss}}][\mathrm{I_{sabc}}] + [\psi_{\mathrm{rabc}}]\} \tag{1.7}$$

Notice the stator phase voltage equation of the three-phase PMSM represented in the three-phase stationary frame (*abc*-axis: three-phase stationary frame) is time varying and nonlinear.

1.4.4 Concordia transform

Now, an equivalent two-phase representation in a fixed frame is introduced.

Using the Concordia transformation

$$\begin{bmatrix} x_{s\alpha} \\ x_{s\beta} \end{bmatrix} = \mathrm{Co}^T \begin{bmatrix} x_{sa} \\ x_{sb} \\ x_{sc} \end{bmatrix} \tag{1.8}$$

Where

$$\mathrm{Co} = \sqrt{\frac{2}{3}} \begin{bmatrix} 1 & 0 \\ -\frac{1}{2} & \frac{\sqrt{3}}{2} \\ -\frac{1}{2} & -\frac{\sqrt{3}}{2} \end{bmatrix} \tag{1.9}$$

multiplying by $\mathrm{C_o}$ the left side of Eq. (1.7) and using the identity $\mathrm{C_o}^T\,\mathrm{Co} = I2{\times}2$ with *x* a variable (voltage, current or flux), it follows that

$$[V_{s\alpha\beta}] = \quad R_s[I_{s\alpha\beta}] + \frac{d[\Lambda_{ss}]}{dt}[I_{s\alpha\beta}] + [\Lambda_{ss}]\frac{d[I_{s\alpha\beta}]}{dt} + \frac{d[\Psi_{r\alpha\beta}]}{dt} \tag{1.10}$$

With $[\Lambda_{ss}] = \{\mathrm{Co}^T[\mathrm{L}_{ss}]\mathrm{Co}\}$.

Taking $M_{so} = -\frac{1}{2}L_{so}$ and using the following trigonometric equivalences:

$$\cos(p\theta_m - 2\pi/3) = \cos(p\theta_m)\cos(2\pi/3) + \sin(p\theta_m)\sin(2\pi/3)$$

and

$$\cos(p\theta_m + 2\pi/3) = \cos(p\theta_m)\cos(2\pi/3) - \sin(p\theta_m)\sin(2\pi/3)$$

Where $\cos(2\pi/3) = -\frac{1}{2}$ and $\sin(2\pi/3) = \sqrt{3}/2$, it follows that

$$[\Lambda_{ss}] = \frac{3}{2}L_{sv}\begin{bmatrix} \cos(2\mathrm{p}\theta_\mathrm{m}) & \sin(2\mathrm{p}\theta_\mathrm{m}) \\ \sin(2\mathrm{p}\theta_\mathrm{m}) & \cos(2\mathrm{p}\theta_\mathrm{m}) \end{bmatrix} + \frac{3}{2}\mathrm{L_{so}}\begin{bmatrix} 1 & 0 \\ 0 & 1 \end{bmatrix} = \begin{bmatrix} L_\alpha & L_{\alpha\beta} \\ L_{\alpha\beta} & L_\beta \end{bmatrix} \tag{1.11}$$

whose the time derivative is given by

$$\frac{d[\Lambda_{ss}]}{dt} = L_{sv} p\Omega \begin{bmatrix} -\sin(2p\theta_m) & \cos(2p\theta_m) \\ \cos(2p\theta_m) & \sin(2p\theta_m) \end{bmatrix} \tag{1.12}$$

Furthermore, using the Concordia transformation, the fluxes $\Psi_{r\alpha}$ and $\Psi_{r\beta}$ can be expressed as:

$$\begin{bmatrix} \Psi_{r\alpha} \\ \Psi_{r\beta} \end{bmatrix} = Co^T \begin{bmatrix} \Psi_{ra} \\ \Psi_{rb} \\ \Psi_{rc} \end{bmatrix} \tag{1.13}$$

$$= \sqrt{\frac{2}{3}} \begin{bmatrix} 1 & -\frac{1}{2} & -\frac{1}{2} \\ 0 & \frac{\sqrt{3}}{2} & -\frac{\sqrt{3}}{2} \end{bmatrix} \Psi_r \begin{bmatrix} \cos(p\theta_m) \\ \cos\left(p\theta_m - \frac{2\pi}{3}\right) \\ \cos\left(p\theta_m + \frac{2\pi}{3}\right) \end{bmatrix} \tag{1.14}$$

It follows that

$$\begin{bmatrix} \Psi_{r\alpha} \\ \Psi_{r\beta} \end{bmatrix} = \sqrt{\frac{3}{2}} \Psi_r \begin{bmatrix} \cos(p\theta_m) \\ \sin(p\theta_m) \end{bmatrix} \tag{1.15}$$

Where $\mathcal{J} = \begin{bmatrix} 0 & 1 \\ -1 & 0 \end{bmatrix}$ is a skew-symmetric matrix, satisfying the following property:

$$\mathcal{J}^T \mathcal{J} = I$$

The time derivative of (1.15) is of the form

$$\begin{bmatrix} \frac{d\Psi_{r\alpha}}{dt} \\ \frac{d\Psi_{r\beta}}{dt} \end{bmatrix} = \begin{bmatrix} -p\Omega\Psi_{r\beta} \\ p\Omega\Psi_{r\alpha} \end{bmatrix} \tag{1.16}$$

1.4.5. Transformation from a Fixed to a Rotating *(d, q)* Frame

To derive an equivalent two-phase representation in order to facilitate the analysis and control design, the Park transformation is usually employed to obtain the expression of the model in the *(d, q)* frame. This transformation renders simpler the dynamical equations of the PMSM.

As introduced previously in this chapter, this method is divided into two steps:

1. *Three-phase-Two-phase Transformation*: from an *(a, b, c)* three-phase stationary frame to an *(α, β)* two-phase stationary frame. This transformation is called the Concordia (obtained from Park transformation preserving energy) or Clarke transformation (obtained from Park transformation preserving amplitudes).
2. *Fixed frame-Rotating frame Transformation*: from an *(α, β)* two-phase stationary frame to a two-phase synchronous rotating *(d, q)* frame, this transformation is called the Park transformation.

By applying the first transformation, i.e., the Concordia transformation Co, then the second step is the application of the Park transformation P in order to obtain the two-phase synchronous rotating representation of the PMSM.

The resulting voltage equations are given as

$$\begin{bmatrix} x_{sd} \\ x_{sq} \end{bmatrix} = \mathrm{P}(\theta_e)^T \begin{bmatrix} x_{s\alpha} \\ x_{s\beta} \end{bmatrix} \tag{1.17}$$

Where

$$\mathrm{P}(\theta_e) = \begin{bmatrix} \cos\theta_e & -\sin\theta_e \\ \sin\theta_e & \cos\theta_e \end{bmatrix},$$

$\theta_e = p\theta_m$ is the electrical angle defined from the position of the rotor with respect to stator.

Then,

$$\begin{bmatrix} x_{sd} \\ x_{sq} \end{bmatrix} = \mathrm{P}(\theta_e)^T \begin{bmatrix} x_{s\alpha} \\ x_{s\beta} \end{bmatrix} = \mathrm{P}(\theta_e)^T \mathrm{Co}^T \begin{bmatrix} x_{sa} \\ x_{sb} \\ x_{sc} \end{bmatrix} \tag{1.18}$$

Combining Eq. (1.18) with (1.7), it follows that

$$\begin{aligned} \mathrm{CoP}(\theta_e)\mathrm{P}(\theta_e)^T \mathrm{Co}^T [V_{sabc}] = \; & R_s \mathrm{CoP}(\theta_e)\mathrm{P}(\theta_e)^T \mathrm{Co}^T [I_{sabc}] + \frac{d}{dt}\{[\Psi_{rabc}]\} \\ & + \frac{d}{dt}\{[\mathrm{L}_{ss}]\mathrm{CoP}(\theta_e)\mathrm{P}(\theta_e)^T \mathrm{Co}^T [I_{sabc}]\} \end{aligned} \tag{1.19}$$

Then obtain the model of the PMSM in the *(d, q)* frame

$$\begin{aligned} [V_{sdq}] = \; & R_s [I_{sdq}] + P(\theta_e)^T \frac{d}{dt}\{[\Lambda_{ss}]P(\theta_e)\}[I_{sdq}] \\ & + P(\theta_e)^T [\Lambda_{ss}]P(\theta_e) \frac{d}{dt}\{[I_{sdq}]\} - p\Omega\mathcal{J}[\Psi_{rdq}] \end{aligned} \tag{1.20}$$

In case of IPMSM the voltage equation is given as:

$$[V_{sdq}] = \{[R_s] - p\Omega[L_{dq}]\mathcal{J}\}[I_{sdq}] + [L_{dq}]\frac{d[I_{sdq}]}{dt} - p\Omega\mathcal{J}[\Psi_{rdq}] \tag{1.21}$$

Moreover, for a specific value of θ_e, the q-component of the rotor flux equal to zero (i.e., $\Psi_{rq} = 0$) and the d-component of the rotor flux equal to Ψ_r, ($\Psi_{rd} = \Psi_r$), it follows that

$$\begin{bmatrix} \mathrm{V_{sd}} \\ \mathrm{V_{sq}} \end{bmatrix} = \begin{bmatrix} \mathrm{R_s} & -\mathrm{p\Omega L_q} \\ \mathrm{p\Omega L_d} & \mathrm{R_s} \end{bmatrix} \begin{bmatrix} \mathrm{i_{sd}} \\ \mathrm{i_{sq}} \end{bmatrix} + \begin{bmatrix} \mathrm{L_d} & 0 \\ 0 & \mathrm{L_q} \end{bmatrix} \begin{bmatrix} \frac{\mathrm{di_{sd}}}{\mathrm{dt}} \\ \frac{\mathrm{di_{sq}}}{\mathrm{dt}} \end{bmatrix} - \begin{bmatrix} 0 \\ \mathrm{p\Omega\Psi_r} \end{bmatrix} \tag{1.22}$$

1.4.6. Mechanical Equations

The rotor electrical position θ_e is determined by this equation

$$\frac{d\theta_e}{dt} = \omega \tag{1.23}$$

And the rotor speed Ω

$$J\frac{d\Omega}{dt} + f_v\Omega = T_e - T_l \tag{1.24}$$

Where:

ω = pΩ, the angular electrical speed,

p: the pole pair number,

Ω: the rotor angular speed,

T_e: the electromagnetic torque

T_l: the load torque,

J: the inertia moment, i.e., the inertia of the synchronous machine plus the load inertia

fv : the viscous friction coefficient.

The electromagnetic torque T_e is generated by the interaction between the rotor magnets poles and the poles induced by the magnetomotive forces in the air gap.

Then, the electromagnetic torque *Te* is given in case of IPMSM as [3]:

$$T_e = p(L_d - L_q)i_{sd}i_{sq} + p(\Psi_{rd}i_{sq} - \Psi_{rq}i_{sd}) \tag{1.25}$$

By replacing (1.25) in (1.24), then

$$J\frac{d\Omega}{dt} + f_v\Omega = p(L_d - L_q)i_{sd}i_{sq} + p(\Psi_{rd}i_{sq} - \Psi_{rq}i_{sd}) - T_l \tag{1.26}$$

Choosing the orientation of the (d, q) frame such that the q-component of the rotor flux is equal to zero ($\Psi_{rq} = 0$) and the d-component of the rotor flux is equal to Ψ_r, then (1.26) can be expressed as follows:

$$J\frac{d\Omega}{dt} + f_v\Omega = p\left(L_d - L_q\right)i_{sd}i_{sq} + p\Psi_r i_{sq} - T_l \tag{1.27}$$

The final model of the IPMSM, in the rotor flux oriented (d, q) frame is

$$\begin{aligned}
\frac{di_{sd}}{dt} &= -\frac{R_s}{L_d}i_{sd} - p\Omega\frac{L_q}{L_d}i_{sq} + \frac{v_{sd}}{L_d} \\
\frac{di_{sq}}{dt} &= -\frac{R_s}{L_q}i_{sq} + p\Omega\frac{L_d}{L_q}i_{sd} + \frac{v_{sq}}{L_q} - p\Omega\frac{\Psi_r}{L_q} \\
\frac{d\Omega}{dt} &= -\frac{f_v}{J}\Omega + \frac{1}{J}p\left(L_d - L_q\right)i_{sd}i_{sq} + p\Psi_r i_{sq} - \frac{1}{J}T_l
\end{aligned} \tag{1.28}$$

For the SPMSM, the stator inductances in the d-axis and q-axis are the same ($L_d = L_q = L_s$). Then, the electromagnetic torque is only given as

$$T_e = p\Psi_r i_{sq} \tag{1.29}$$

Replacing (1.29) in (1.24) with Ld = Lq = Ls, it follows that the rotor speed dynamics is given as

$$J\frac{d\Omega}{dt} = -f_v\Omega + p\Psi_r i_{sq} - T_l \tag{1.30}$$

Then the final SPMSM model in the rotor flux oriented (d,q) frame, is

$$\begin{aligned}
\frac{di_{sd}}{dt} &= -\frac{R_s}{L_s}i_{sd} + p\Omega i_{sq} + \frac{v_{sd}}{L_s} \\
\frac{di_{sq}}{dt} &= -\frac{R_s}{L_s}i_{sq} - p\Omega i_{sd} + \frac{v_{sq}}{L_s} - p\Omega\frac{\Psi_r}{L_s} \\
\frac{d\Omega}{dt} &= -\frac{f_v}{J}\Omega + \frac{p\Psi_r}{J}i_{sq} - \frac{1}{J}T_l
\end{aligned} \tag{1.31}$$

1.4.7. State space model in the *(d, q)* Frame

For the torque or angular speed control, the nonlinear state-space model of the IPMSM in the *(d, q)* frame, is given as

$$\begin{bmatrix} \frac{di_{sd}}{dt} \\ \frac{di_{sq}}{dt} \\ \frac{d\Omega}{dt} \end{bmatrix} = \begin{bmatrix} -\frac{R_s}{L_d} i_{sd} + \frac{pL_q}{L_d} i_{sq}\Omega \\ -\frac{R_s}{L_q} t_{sq} - \frac{pL_d}{L_q} i_{sd}\Omega - \frac{p\Psi_r}{L_q}\Omega \\ \frac{p\Psi_r}{J} i_{sq} - \frac{p(L_q - L_d)}{J} i_{sd} i_{sq} - \frac{f_v}{J}\Omega \end{bmatrix} + \begin{bmatrix} \frac{1}{L_d} & 0 & 0 \\ 0 & \frac{1}{L_q} & 0 \\ 0 & 0 & -\frac{1}{J} \end{bmatrix} \begin{bmatrix} v_{sd} \\ v_{sq} \\ T_l \end{bmatrix} \quad (1.32)$$

where

$[i_{sd}\ ,\ i_{sq}\ ,\Omega]$ are the states

$[v_{sd},\ v_{sq}\ ,\ T_l\ ]$ are the inputs, where T_l is assumed to be an unknown input.

The measurable output are the stator currents $[i_{sd}\ ,\ i_{sq}\ ]$.

If the permanent magnet synchronous machine is without salient poles (SPMSM case), i.e., the inductances in *d*-axis and *q*-axis are equal ($L_d = L_q = L_s$).

1.5. Voltage source Inverter Feeding a Permanent-Magnet Synchronous Motor

Fig.1.5 show the PMSM drive, it consists of a diode rectifier, DC link filter and an inverter. The rectifier converts supply AC voltage into DC voltage. The DC voltage is filtered by a capacitor in the DC link. The inverter converts the DC to a variable voltage, variable frequency AC for motor speed or (torque/current) control.

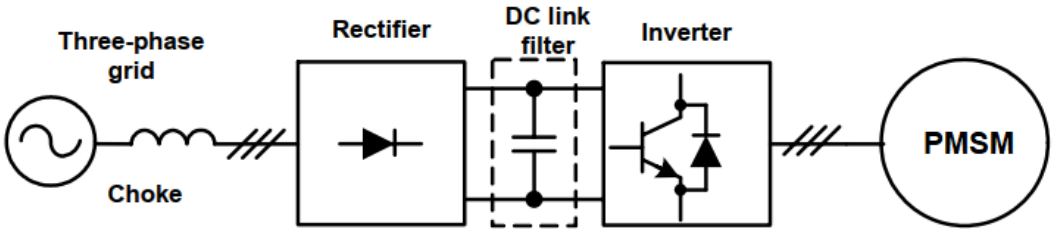

Fig.1.5: Basic scheme of adjustable speed AC motor system.

Fig.1.6 below shows a simplified scheme of the two-level bridge topology of the voltage source inverter. The PMSM is supposed as a star-connected three phase balanced load.

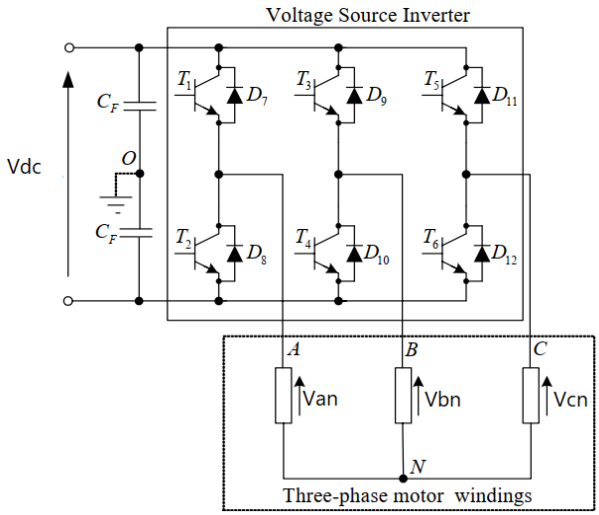

Fig.1.6: Basic scheme of voltage source inverter circuit.

The one leg of inverter consists of two transistor switches. A simple transistor switch consists of feedback diode connected in anti-parallel with transistor. Feedback diode conducts current when the load current direction is opposite to the voltage direction.

The inverter's control bases on the logic values S_i, where:

S_i=1, T_i is ON and $\overline{T_i}$ is OFF.

S_i=0, T_i is OFF and $\overline{T_i}$ is ON.

with: i= *a, b, c.*

The voltage vector is generated by the following equation

$$V_s = \sqrt{\frac{2}{3}} V_{dc} \left[S_a + S_b e^{j\frac{2\pi}{3}} + S_c e^{j\frac{4\pi}{3}} \right] \qquad (1.33)$$

V_{dc}*:* is the DC link voltage

There are eight possible positions from the combinations of switching states. Six are active vectors (V1, V2 … V6) and two are zero vectors (V0, V7). These eight switching states are shown as space vectors in **Fig.1.7**:

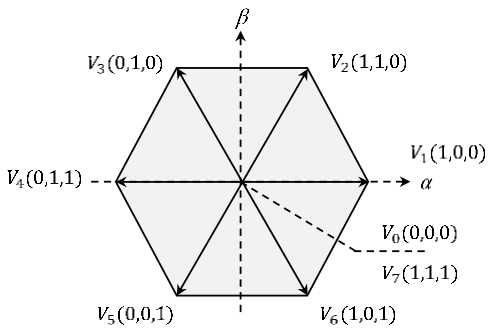

Fig.1.7: VSI Voltage vectors in the complex plane

1.6. Conclusion

In this chapter, an overview of permanent magnet synchronous machine has been first given. In particular, it's structure, different designs and main application.

Then this chapter present the model that allow to describe the dynamical behavior of the PMSM have been introduced. These models have been expressed either in a fixed *(α, β)* frame or in a rotating *(d, q)* frame in order to describe the dynamical behavior of this machine.

Moreover, this chapter has been introduced the structure and the principle of operation of the voltage source inverter (VSI) that feed the permanent magnet synchronous motor. Then main purpose of feeding the PMSM with VSI is to have a variable speed operation, which is the aim of our next chapter.

Contents

2.1. Introduction

Generally, the control of induction machines in variable speed operation is more complicate than in DC machines. The main reasons are that they have more complex dynamic and more request of complicated calculations. The vector control and direct torque control (DTC) are the most known control algorithms in literature for variable-speed AC motors. DTC strategy was introduced in the middle of the 80s as an alternative of field-oriented control (FOC) because of many advantages, such as simpler structure, faster dynamic response and less dependence to machine parameters [4]. However, the basic DTC strategy has a variable switching frequency due to the use of hysteresis controllers, consequently, they cause non-desired ripples in flux and torque. The insertion of space vector modulation strategy (SVM) in DTC scheme is among the proposed solutions to overcome these drawbacks, where SVM can reduce the ripples by providing a constant switching.

Therefore, this chapter a comparative study between the conventional direct torque control and the improved direct torque control with constant switching frequency using the space vector modulation.

2.2. Overview about variable frequency drives

AC machines have to be driven by a Variable Frequency Drive (VFD) to be able to run at different speeds. Control methods for electric motors can be divided into two main categories depending of what quantities they control (Fig.2.1). The control algorithm Scalar Control controls only magnitudes, whereas the algorithms Vector Control controls both magnitude and angles.

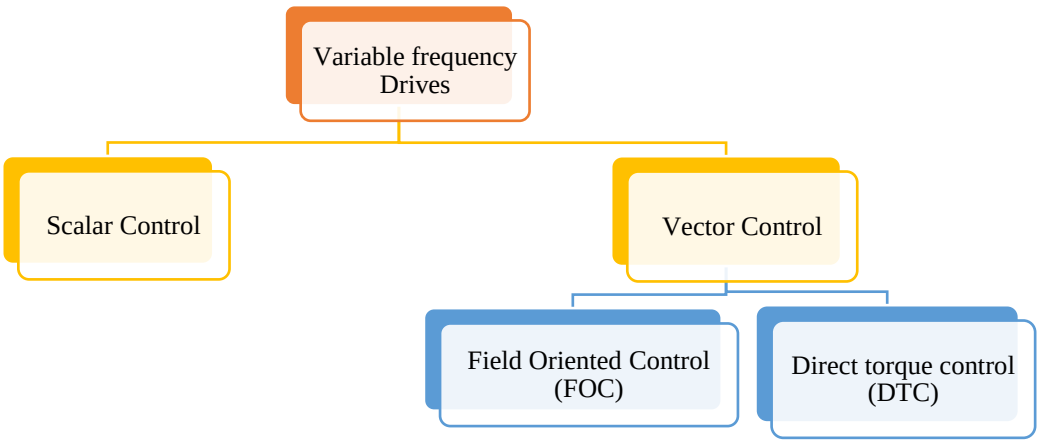

Fig.2.1 Classification of variable frequency control strategies

The most popular method of vector control is known by the Field-Oriented Control (FOC) which was proposed at the beginning of 1970s by Hasse and Blaschke

[5; 6]. In the middle of 1980s, another method is presented by Takahashi and Depenbrock [7; 8] which is called the Direct Torque Control.

2.2.1. Scalar control

The Scalar control (*V/f*) which is known also by Volt/Hertz control is a simple technique used to control the speed of the induction Motors. The main concept of *V/f* is to keep the ratio of the stator voltage to frequency constant to maintain constant maximum available torque.

2.2.2. Field oriented control

On the contrary to the scalar control, the field-oriented control scheme bases on the dynamic model the machine which makes it valid for both steady and transient states. In spite of the coupled and nonlinear nature of the induction machine, FOC can control it as a separate excitation DC machine which is featured by a nature decoupling. FOC achieves a similar behavior by transforming all quantities to a rotating synchronous frame (*d, q*) where they appear as DC quantities.

2.3. Conventional direct torque control of PMSM

Direct Torque Control was first introduced for induction motors (IM) [9] in 1984 and the Direct Self Control method [10] in 1985. The methods were characterized by their simplicity, good performance and robustness. Unlike the FOC method, DTC worked without any external measurement of the rotors mechanical position. The reason behind the simplicity is that DTC not require any current regulators, transformations to rotating reference frame or PWM generators.

Direct torque control achieves a decoupled control of the stator flux and the electromagnetic torque in the stationary frame (α, β). It uses a switching table for the selection of an appropriate voltage vector. The selection of the switching states is related directly to the variation of the stator flux and the torque of the machine. Hence, the selection is made by restricting the flux and torque magnitudes within two hysteresis bands. Those controllers ensure a separated regulation of both of these quantities. The inputs of hysteresis controllers are the flux and the torque errors as well as their outputs determine the appropriate voltage vector for each commutation period [11].

2.3.1. PMSM model presentation

The voltage and flux linkage equations of PMSM are got in the ($\alpha -\beta$) coordinate.

$$\begin{cases} V_\alpha = R_s i_\alpha + L_s \frac{di_\alpha}{dt} - \omega_r \psi_r \sin\ \theta_r \\ V_\beta = R_s i_\beta + L_s \frac{di_\beta}{dt} + \omega_r \psi_r \cos\ \theta_r \end{cases} \quad (2.1)$$

$$\begin{cases} \frac{d\psi_{s\alpha}}{dt} = -R_s i_{s\alpha} + V_{s\alpha} \\ \frac{d\psi_{s\beta}}{dt} = -R_s i_{s\beta} + V_{s\beta} \end{cases} \quad (2.2)$$

The electromagnetic torque T_e is given by:

$$T_e = \frac{3}{2} p_m \left(\psi_{s\alpha} i_{s\beta} - \psi_{s\beta} i_{s\alpha}\right) \quad (2.3)$$

2.3.2. The control of the amplitude of stator flux linkage

The stator flux linkage in the α-β stationary reference frame can be expressed as**:**

$$\psi_s = \int (V_s - R_s i_s) dt \quad (2.4)$$

During the switching interval, every voltage vector can be regarded as constant, and equation can be rewritten as:

$$\psi_s = V_s t - R_s \int i_s dt + \psi_{s|t=0} \quad (2.5)$$

where $\psi_{s|t=0}$ is the initial stator flux linkage.

The equation implies that ψ_s will move in the direction of the applied voltage vector if the stator resistance is neglected. Therefore, the amplitude of stator flux linkage can be increased or decreased by selecting the proper voltage vector. **Fig. 2.2** shows how the voltage vectors are selected for keeping ψ_s within a hysteresis band $|\Delta\psi_s|$. There are six independent sectors setting in the whole vector plane (θ_i , *i = 1– 6*).

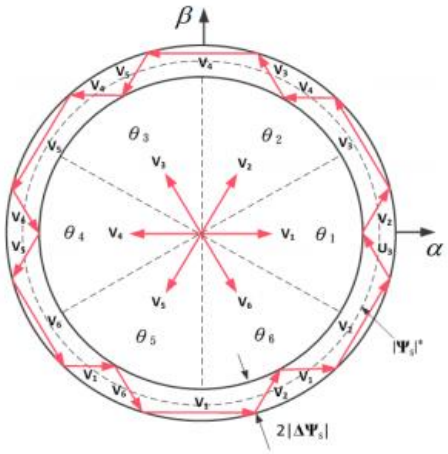

Fig. 2.2: Control of the amplitude of stator flux linkage.

A two-level hysteresis comparator is used for flux regulation. It allows to drop easily the flux vector extremity within the limits of the two concentric circles with close radius, as shown in **Fig.2.3.** The choice of the hysteresis bandwidth h_{ψ_s} depends on the switching frequency of the inverter [12; 13].

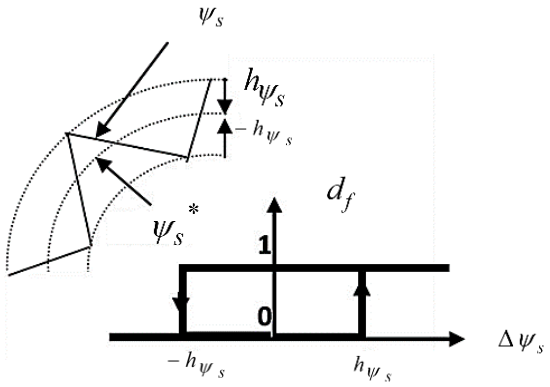

Fig.2.3: Tow-level hysteresis comparator for stator flux control.

The logical outputs of the flux controller are defined as:

$$\begin{cases} d_f = 1 & if\ \Delta\psi_s > h_{\psi_s} \\ d_f = 0 & if\ \Delta\psi_s \le -h_{\psi_s} \end{cases} \quad (2.6)$$

h_{ψ_s} is hysteresis band of stator flux

The stator flux error is defined by the difference between the references value of flux and the actual estimated value:

$$\Delta\psi_s = |\psi_s^*| - |\psi_s| \quad (2.7)$$

2.3.3. Control of electromagnetic torque

During one sampling period, the rotor flux vector is supposed invariant. The torque of PMSM can be expressed as follows:

$$T_e = \frac{3p_m}{2L_s}|\psi_s|\psi_f \sin\ \delta \quad (2.8)$$

where:

p is the number of poles pairs.

ψ_s, ψ_r are stator and rotor flux vectors.

δ angle between the stator and rotor flux vectors

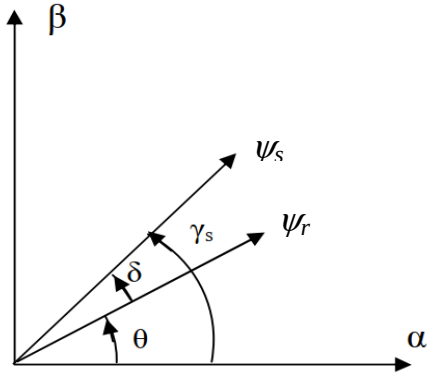

Fig.2.4: Relationship between different quantities in different reference frames.

From expression (2.8), it is clear that the electromagnetic torque is controlled by the stator and rotor flux amplitudes. If those quantities are maintaining constant, the torque can be controlled by adjusting the load angle δ (**Fig.2.4**).

The torque regulation can be realized using three-level hysteresis comparator **(Fig.2.5)**. It allows to control the motor in both rotation senses. The tow-level comparator can be used for one rotation sense.

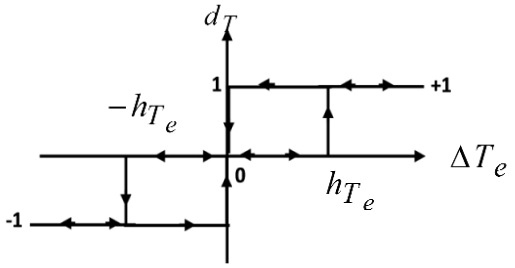

Fig.2.5 Three level hysteresis comparator for electromagnetic torque control.

The logical outputs of the torque controller are defined as:

$$\begin{cases} d_T = 1 & if\ \Delta T_e > h_{T_e} \\ d_T = 0 & if\ -h_{T_e} \le \Delta T_e \le h_{T_e} \\ d_T = -1 & if\ \Delta T_e < -h_{T_e} \end{cases} \quad (2.9)$$

h_{T_e} is hysteresis band of torque.

The torque error is defined by the difference between the references values of the torque and the actual estimated values:

$$\Delta T_e = T_e^* - T_e \quad (2.10)$$

2.3.4. Flux and torque estimation

Accurate flux estimation in PMSM is required to have proper drive operation, it's stability. Most of the flux estimation techniques known is based upon voltage modeling, current modeling, or combination of both of these. The estimation based upon current is generally applied at low frequency, and the knowledge of the stator current and rotor mechanical speed or position is required in this case.

$$\psi_{\alpha\beta,est} = \int \left(V_{\alpha\beta} - R_s i_{\alpha\beta}\right) dt \quad (2.11)$$

The electromagnetic torque is estimated by:

$$T_e = \frac{3}{2} p\left(\psi_{s\alpha} i_{s\beta} - \psi_{s\beta} i_{s\alpha}\right) \quad (2.12)$$

2.3.5. Currents and Voltage Transform

The measured motor currents are calculated with the Clarke transform from *abc* phase reference frame into the $\alpha\beta$ reference frame.

The stator currents components $i_{s\alpha}$, $i_{s\beta}$ can be obtained also by applying Concordia transformation on the measured currents:

$$\begin{cases} i_{s\alpha} = \sqrt{\frac{2}{3}} i_{sa} \\ i_{s\beta} = \frac{1}{\sqrt{2}} \left(i_{sb} - i_{sc} \right) \end{cases} \tag{2.13}$$

The voltage $V_{\alpha\beta}$ is estimated from the inverters switching state and the DC-link voltage in the $\alpha\beta$ reference frame by the voltage equation [14].

$$\begin{cases} V_a = \sqrt{\frac{3}{2}} \cdot V_{dc} \left[S_a - \frac{1}{2} S_b - \frac{1}{2} S_c \right] \\ V_\beta = \frac{1}{\sqrt{2}} \cdot V_{dc} [S_b - S_e] \end{cases} \tag{2.14}$$

Where S_{abc} is the state of the power switches.

2.3.6. Sector Calculation and look-up table

To maintain a decoupled control, pair of hysteresis comparators receives the stator flux and torque errors as inputs. Then, the comparators outputs determine the appropriate voltage vector selection [4; 15]. However, the choice of voltage vector is not only depending on the output of hysteresis controllers, but on the position of stator flux vector also. Thus, the circular stator flux vector trajectory will be divided into six symmetrical sectors [16; 17].

where:

Sector 1: $^{11\pi}/_{6} \le \theta < {}^{\pi}/_{6}$, sector 2: $^{\pi}/_{6} \le \theta < {}^{\pi}/_{2}$ …, sector 6: $^{3\pi}/_{2} \le \theta < {}^{11\pi}/_{6}$

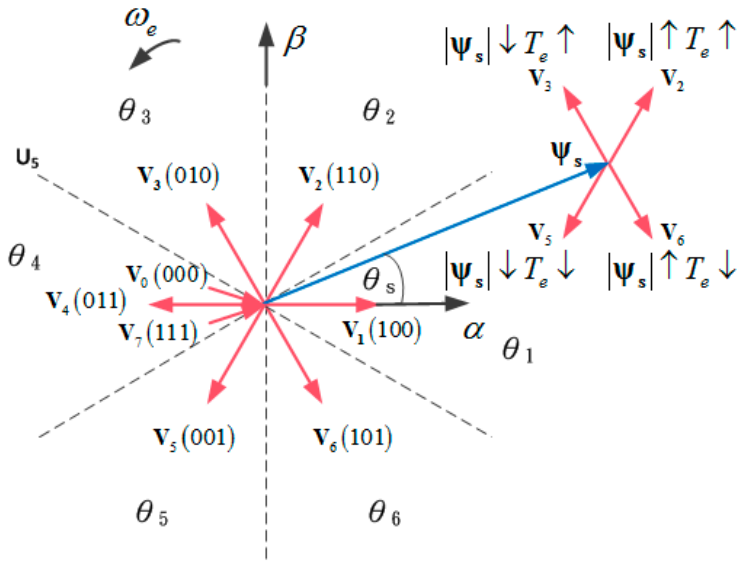

Fig.2.6: Effects of voltage vector on the stator flux and torque.

While the stator flux vector is located in the sector *i* we have [17]:

- If V_{i+1} is selected, ψ_s increases and T_e increases.
- If V_{i-1} is selected, ψ_s increases and T_e decreases.
- If V_{i+2} is selected, ψ_s decreases and T_e increases.
- If V_{i-2} is selected, ψ_s decreases and T_e decreases.

For each sector, the vectors (V_i and V_{i+3}) are not considered because both of them can increase or decreases the torque in the same sector according to the position of flux vector on the first or the second sector [18]. If the zero vectors V_0 and V_7 are selected, the stator flux will stop moving and its magnitude will not change, the electromagnetic torque will decrease, but not as much as when the active voltage vectors are selected [19].

The resulting look-up table for DTC which was proposed by Takahashi is presented in **Table 2.1:**

Error	Sectors	I	II	III	IV	V	VI
d_f=1	d_T=1	V_2	V_3	V_4	V_5	V_6	V_1
	d_T = 0	V_7	V_0	V_7	V_0	V_7	V_0
	d_T = −1	V_6	V_1	V_2	V_3	V_4	V_5
d_f=0	d_T=1	V_3	V_4	V_5	V_6	V_1	V_2
	d_T = 0	V_0	V_7	V_0	V_7	V_0	V_7
	d_T = −1	V_5	V_6	V_1	V_2	V_3	V_4

Table 2.1 Look-up table for basic direct torque control.

2.3.7. Speed Controller

DTC strategy has the ability to operate even without a speed regulation loop, so it doesn't require any information about rotor speed. This can classify DTC as a speed sensorless strategy for many industrial applications. Otherwise, to achieve an adjustable speed control, a speed controller is necessary to have a speed regulation and to generate the reference of electromagnetic torque. Commonly, the proportional-integral (PI) controllers are used for the regulation. It is performed by comparing the speed reference signal to the actual measured speed value. Then the comparison error becomes the input of the PI controller.

The tuning of PI controllers is usually disregarding the physical limitation of the system such as the maximum current and voltage. The used PI controller in our work in the outer speed loop is the anti-windup controller. It allows to enhance speed control performance by cancelling the windup phenomenon which is caused by the saturation of the pure integrator, and for the speed PI controller's gain, the calculations

are shown in the Appendix.A.2. **Fig.2.7** shows the speed anti-windup PI controller diagram block.

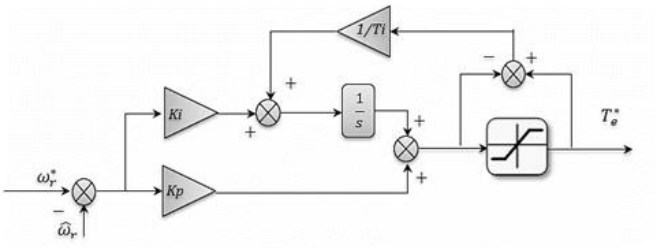

Fig.2.7: Speed anti-windup PI controller.

The global control scheme of basic direct torque control strategy is shown in **Fig.2.8** It is composed of: speed regulation loop using PI controller, decoupled flux and torque hysteresis controllers, look-up switching table, an association of VSI-Induction motor, voltage and current calculation blocks with 3/2 (Concordia) transformation and flux/torque estimators with position/sector determination.

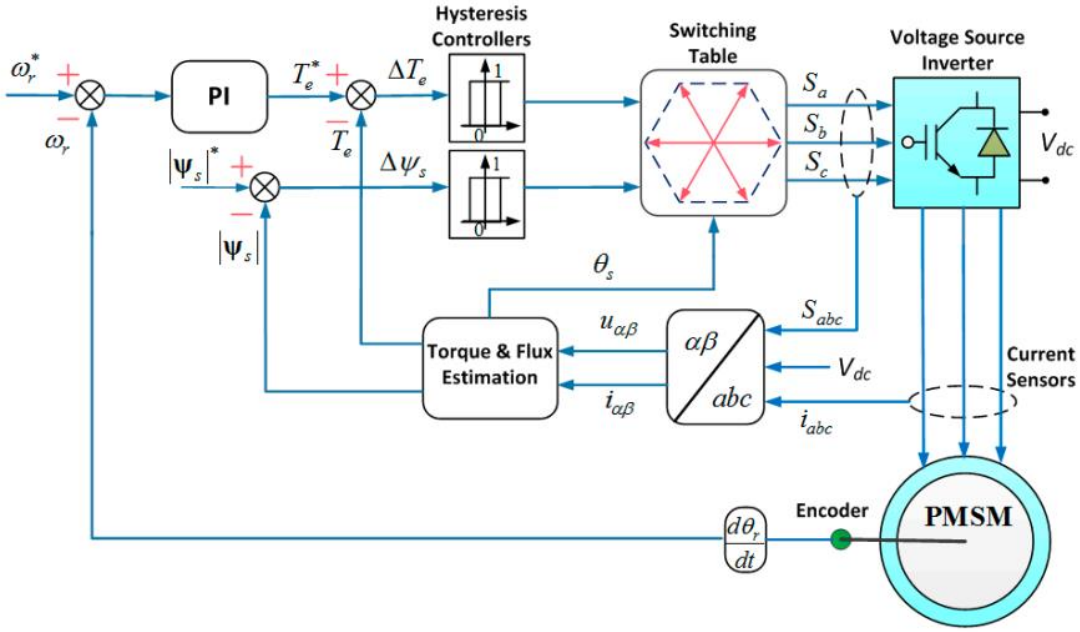

Fig.2.8: Block diagram of the classical direct torque control (DTC) method for PMSM.

2.4. Direct torque control with constant switching frequency

In this DTC strategy, the lookup switching table and the hysteresis comparators are replaced by the space voltage modulation (SVM) for the purpose of voltage vector selection. This control schemes can preserve a constant switching frequency, consequently it reduces the high torque and flux ripples.

The insertion of the space vector modulation (SVM) in DTC control scheme has been discussed also in literature. SVM preserves a constant switching frequency which

can reduce high torque/flux ripples and minimize current harmonic distortion. Consequently, an effective control of the stator flux and torque is achieved. Several SVM-DTC methods have been proposed according to their structures, such as: cascade structure of DTC-SVM scheme and parallel DTC-SVM.

2.4.1. Space vector modulation

SVM is different from the conventional pulse width modulation (PWM). It relies on the space vector representation of the inverter output. There are no separate modulators for each phase. The reference voltages are given by space voltage vector (i.e. voltage vector components in the complex plan) [20]. The principle of SVM is the prediction of inverter voltage vector by the projection of the reference vector V_s^* between adjacent vectors corresponding to two non-zero switching states. [21; 22]. For two-levels inverter, the switching vectors diagram forms a hexagon divided into six sectors, each one is expanded by 60° as shown in **Fig.2.9**.

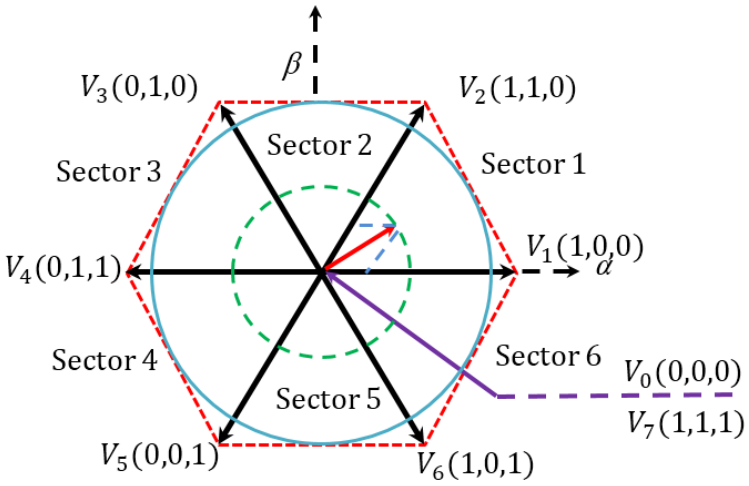

Fig.2.9: Diagram of voltage space vector.

The application time for each vector can be obtained by vector calculations and the rest of the time period will be spent by applying the null vector.

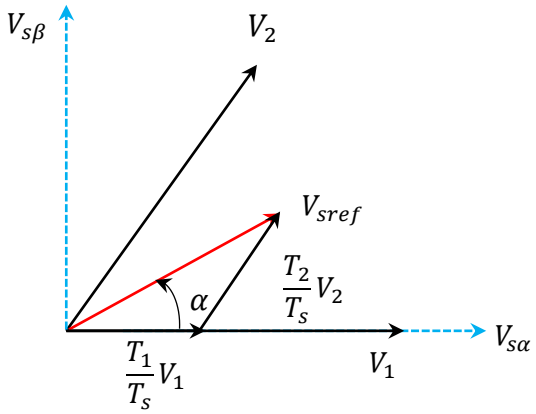

Fig.2.10: Reference vector as a combination of adjacent vectors at sector 1.

When the reference voltage is in sector 1 (**Fig.2.10**), the reference voltage can be synthesized by using the vectors V_1, V_2, and V_0 (zero vector).

The volt-second principle for sector 1 can be expressed by:

$$V_{sref}T_s = V_1T_1 + V_2T_2 + V_0T_0 \tag{2.15}$$

$$T_s = T_1 + T_2 + T_0 \tag{2.16}$$

T_1, T_2 and T_0 are the corresponding application times of the voltage vectors respectively. T_s is the sampling time.

The determination of times T_1 and T_2 corresponding to voltage vectors are obtained by simple projections:

$$\begin{cases} T_1 = \frac{T\sqrt{3}}{\sqrt{2}V_{dc}}\left(V_{\alpha ref} - \frac{V_{\beta ref}}{\sqrt{3}}\right) \\ T_2 = \sqrt{2}\frac{T}{V_{dc}}V_{\beta ref} \end{cases} \tag{2.17}$$

V_{dc}: DC bus voltage.

The calculation of the switching times (duty cycles) is expressed as follows:

Upper side:

$$T_{aon} = T_1 + T_2 + T_0/2 \tag{2.18}$$

$$T_{bon} = T_2 + T_0/2 \tag{2.19}$$

$$T_{con} = T_0/2 \tag{2.20}$$

Lower side:

$$T^*_{aon} = T_0/2 \tag{2.21}$$

$$T^*_{bon} = T_1 + T_0/2 \tag{2.22}$$

$$T^*_{con} = T_1 + T_2 + T_0/2 \tag{2.23}$$

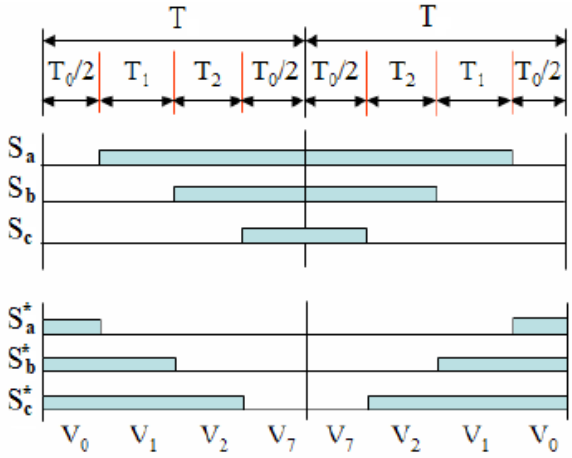

Fig.2.11: Switching times for sector 1

2.4.2. Direct Torque Control Scheme Using Space Vector Modulation (DTC-SVM)

The strategy of the DTC-SVM uses a switching SVM vector and imposed constant frequency. This fixed switching frequency based-DTC does not use the controller hysteresis; it significantly relaxes the constraints of computing time. Furthermore, this methodology is based on an explicit calculation of the control to achieve the objective of torque, and the oscillations of the latter are considerably reduced [14] .

In DTC-SVM, the generation of command pulses (S_a, S_b, S_c)applied to control the inverter switches is usually based on the use of a predictive controller. A flux and voltage calculation bloc receives the reference amplitude stator flux ψ_s^* and the module and the position of estimated stator flux, then it determinates the stator voltage reference ($V_{s\alpha}^*$, $V_{s\beta}^*$) for space vector modulator (SVM), which finally generates the pulses to control the inverter.

The related on between the torque error and the increment of the load angle δ is nonlinear. So, a PI controller that produces the increment of the load angle can minimize the error instantaneous torque.

The reference stator flux vector can be estimated by the polar-rectangular transformation formula which is expressed in the Eq (2.24)

$$\psi_s^* = |\psi_s^*|\cos(\Delta\theta_s + \theta_s) + j|\psi_s^*|\sin(\delta + \theta_s) \quad (2.24)$$

θ_s is the stator flux angle with $\Delta\theta_s = T_s\omega_r p_m + \Delta\delta$

The voltage components $(V_{s\alpha}^*, V_{s\beta}^*)$ are calculated based on the stator flux error $\Delta\psi_s$ and sampling time in (α, β) frame by the following equation:

$$\begin{cases} V_{s\alpha}^* = \dfrac{\Delta\psi_{s\alpha}}{T_s} = \dfrac{\psi_{s\alpha}^* - \hat{\psi}_{s\alpha}}{T_s} + R_s i_{s\alpha} \\ V_{s\beta}^* = \dfrac{\Delta\psi_{s\beta}}{T_s} = \dfrac{\psi_{s\beta}^* - \hat{\psi}_{s\beta}}{T_s} + R_s i_{s\beta} \end{cases} \quad (2.25)$$

The diagram of DTC-SVM control scheme is presented in **Fig.2.12**

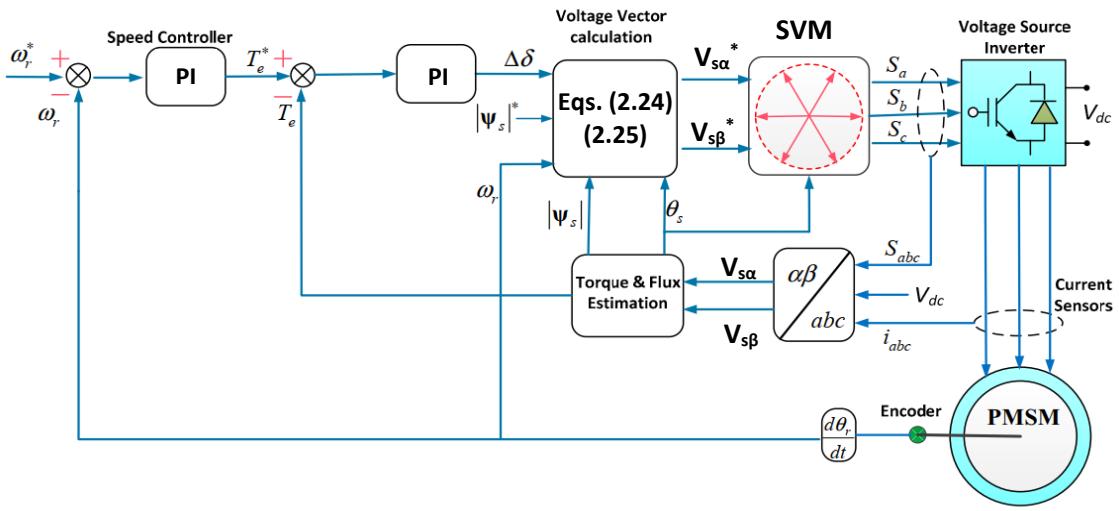

Fig.2.12: Block diagram of SVM-Direct torque control of PMSM.

2.5. Comparative evaluation of direct torque control techniques

The switching table-based DTC is featured by simple decoupled control scheme and fast dynamic torque response, while the direct torque control with space vector modulation combines the advantages of DTC and FOC strategies. According to the mentioned comparative analysis, the following table summarizes the features of the SVM-DTC control scheme compared to the conventional DTC.

Classical DTC with switching table	**SVM-DTC Structures**
+ Fast dynamic torque response.	+ Fast dynamic torque response.
+ No coordinate transformation.	+ No coordinate transformation.
+ No current regulation.	+ No current regulation.
+ Independence on machine parameters.	+ Independence on machine parameters.
– High current and torque and flux ripples.	+ Reduced torque and flux ripples.
– Variable switching frequency.	+ Constant switching frequency.
– High noise levels at low speed operation	+ Good dynamic at low speed operation.
– High switching losses.	+ Low switching losses.

+ Advantages; – Disadvantages

Table.2.2: Advantages of DTC–SVM compared to the classical DTC.

2.6. Conclusion

In this chapter a comparative study between conventional and SVB based DTC strategies has been presented. The main purpose of using space vector modulation in DTC strategy is the reduction of the torque and the flux high ripples. In addition, SVM can preserve a constant switching frequency and can reduce switching losses.

The next chapter will focus in speed regulation improvement in DTC-SVM.

3.1. Introduction

Most physical systems are nonlinear and multivariable, by nature, they have inherent interconnected nonlinearities in their internal dynamics [23]. We take in particular the induction motor. It has control problems in speed adjustable drives contrary to the DC motor due to some reasons [24], such as, the high order of internal coupled nonlinearity, parameters variation because of environment effects and external load perturbations during its operation.

The use of conventional approaches such as the proportional-integral-differential (PID) controllers to understand the behavior of those systems by analytical techniques can be inadequate. This has led to an intense interest in the development of so-called nonlinear and robust control techniques which seeks to solve these problem [25]. Among these techniques, the sliding mode control. This chapter aim to integrate the sliding mode control to enhance the performance of DTC-SVM strategy.

3.2. Sliding Mode Control Theory

The sliding mode control (SMC) is a particular type of variable structure control (VSC). The first concept of SMC appeared in Russian literature (The former Soviet Union) in 1950s and developed by Emelyanov in 1960s [26]. Later, Utkin has written an English summary of papers on the sliding mode control [27]. Due to the implementation difficulties of high-speed switching, this approach didn't receive the attention that it deserved until the 1970s. Then, the sliding mode control theory was widely disseminated to the different areas at the beginning of 1980s.

3.2.1. Basic concepts of SMC

The SMC is a variable structure control method widely known in the automatic and control field. The strength points of the SMC are the robustness against uncertainties, fast response and simple software and hardware implementation [28; 29]. SMC bases on forcing the system trajectory to slide along a switching surface by determined control law. It consists of two phases, a reaching phase where the state trajectory is driven to the surface $s = 0$ and reaches it in a finite time, followed by a sliding phase where it slides on the switching surface to an equilibrium point, as shown in Fig.3.1 [30].

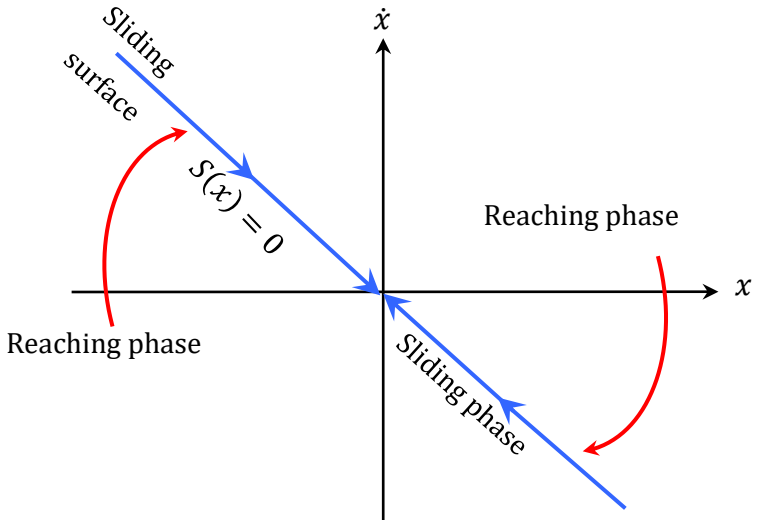

Fig.3.1: Sliding mode principle of state trajectory.

3.2.2. Sliding surface choice

The design of SMC can be achieved into two phases. The first phase is determining the switching surface. In engineering applications, the error between control objectives and the reference input and its derivative is used to form the sliding surface [31].

The second phase is to design the control law in a way that to steer the system trajectory to the sliding surface [32; 33]. The well applied sliding surface was proposed by Slotine as:

$$S = \left(\frac{d}{dt} + \lambda \right)^{n-1} e \tag{3.1}$$

Where S is the sliding surface, λ is positive constant, e is the system error and n is the system relative order.

3.2.3. Existence Conditions of sliding mode control

The sliding mode must exist in all points of the surface $S = 0$. To guarantee that the system state stays in sliding mode after reaching mode, the existence conditions should be [34; 24]:

$$\begin{cases} \lim\limits_{S \to 0^-} \dot{S} > 0 \\ \lim\limits_{S \to 0^+} \dot{S} < 0 \end{cases} \tag{3.2}$$

It means that if *S* is positive, then its derivative should be negative and if *S* is negative, then its derivative should be positive. It can be written in a simplified way as:

$$S\dot{S} < 0 \tag{3.2}$$

Since the existence problem looks like a generalized stability problem, it can be summarized in terms of Lyapunov's theory as follows [35; 36]:

$$V = \frac{1}{2}S^2 \tag{3.3}$$

The aim is to determine a control law such that $\dot{V} < 0$ in order to drive the system states to the sliding-mode surface:

$$\dot{V} = S\dot{S} < 0 \tag{3.4}$$

when $S \neq 0$, $\dot{V} < 0$ is negative definite. Therefore, for finite time convergence the condition (3.4) ensure asymptotically convergence towards the sliding surface.

3.2.4. Control design

The most common method of SMC is relay control, the equivalent control scheme and the linear feedback with switched gains. The equivalent control is the most used structure for the control of electrical machines (**Fig.3.2**). It is preferred due to the relay control which is more suitable for the structure of the power electronics converters [37].

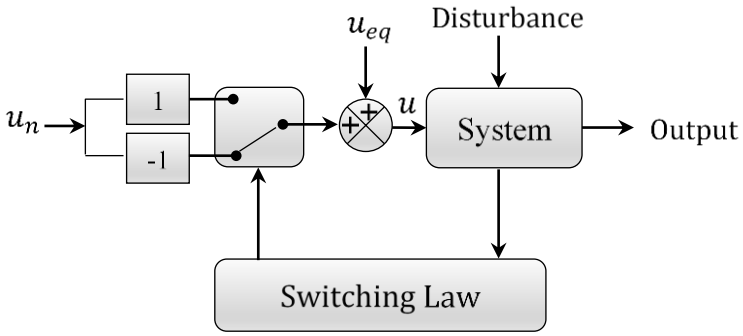

Fig.3.2: Equivalent control structure.

The design of sliding mode control is mostly performed by two parts. The equivalent control u_{eq} is added to another control term called the discontinues control u_n in order to ensure that the state trajectory reaches and stays on the switching surface.

The control law expression is given by:

$$u = u_{eq} + u_n \tag{3.5}$$

By considering the following state system:

$$\dot{x} = A(x) + B(x)\,\mathrm{u} \tag{3.6}$$

The equivalent control is defined during the sliding phase and the steady state where $S = \dot{S} = 0$ and $u_n=0$ [36].

$$u_{eq} = -\left(\frac{\partial S}{\partial x} B(x)\right)^{-1} \frac{\partial S}{\partial x} A(x) \tag{3.7}$$

The existence of an inverse matrix is a necessary, which means the next condition (3.8):

$$\frac{\partial S}{\partial x} B(x) \neq 0 \tag{3.8}$$

the derivative of new sliding surface expression becomes:

$$\dot{S} = \frac{\partial S}{\partial x} B(\mathrm{x})\,\mathrm{u_n} \tag{3.9}$$

The discontinuous control u_n is determined during the convergence state and must guarantee the finite time convergence condition $S\dot{S} < 0$ which is given by:

$$S\dot{S} = S\,\frac{\partial S}{\partial x} B(\mathrm{x})\,\mathrm{u_n} < 0 \tag{3.10}$$

In order to satisfy this condition, the sign of u_n must be the opposite of the sign of $S\,\frac{\partial S}{\partial x} B(\mathrm{x})$. The discontinuous control is defined as a switching term formed by relay function *sign(S)* (**Fig.3.3**) multiplied by a constant coefficient *K*.

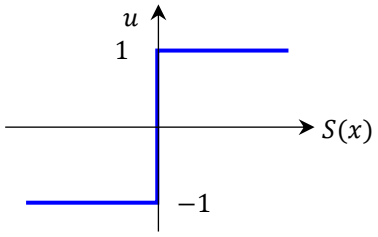

Fig.3.3: Function *sign(s)*.

The relay function is defined by:

$$sign(S) = \begin{cases} +1 & if \quad S \geq 0 \\ -1 & if \quad S < 0 \end{cases} \tag{3.11}$$

$$u_n = -K\,sign(S) \tag{3.12}$$

The coefficient *K* must be positive to ensure the convergence condition.

In general, the strengths of SMC can be concluded:

- Low sensitivity to plant parameter uncertainty.

- Greatly reduced-order modeling of plant dynamics.
- Finite-time convergence (due to discontinuous control law).

3.2.5. Chattering phenomenon

The main drawback of the SMC is the chattering phenomenon which is caused by an infinite commutation due to the depending on the switching function relay (*sign(s)*) (**Fig.3.3**) in the control design. The disagreeable chattering phenomenon can excite high frequency harmonics and can also lead to damage of moving mechanical parts and heat losses in the electrical parts.

The common solution of this problem is to replace the classical *sign(s)* function by smoother switching functions, such as *saturation* function (*sat(s)*) [38] and *sigmoid* (*sigm(s)*) function [39] as shown in **Fig.3.4**.

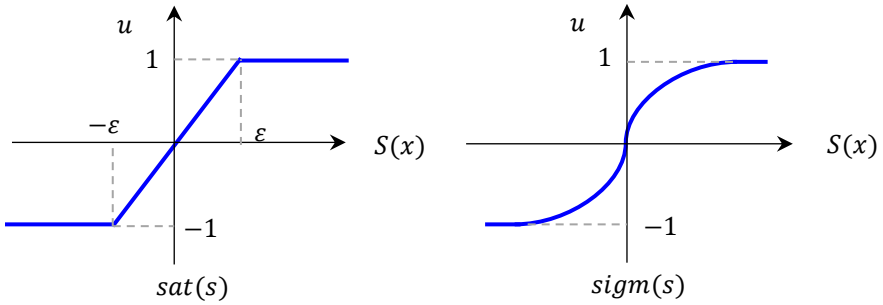

Fig.3.4: Saturation and sigmoid functions.

The shown functions are defined by:

$$sat(s) = \begin{cases} 1 \ if \ x > \varepsilon \\ \dfrac{x}{\varepsilon} \ if \ |x| \le \varepsilon \\ -1 \ if \ x < -\varepsilon \end{cases} \tag{3.13}$$

$$sigm(s) = \left(\frac{2}{1+e^{qs}} \right) - 1 \tag{3.14}$$

Where:

ε is a small positive constant representing the width of boundary layer.

q is a small positive constant which adjusts the sigmoid function slope.

3.3. High order sliding mode control

The higher order sliding mode control is another method used to eliminate the problem of chattering. It is a generalized idea of the first order which based on higher order

derivatives of the sliding surface. Besides keeping the same robustness and performance of the conventional sliding mode control (i.e., fast response and high robustness) it can reduce considerably the effect of chattering.

The n^{th} sliding mode order can be determined by:

$$s = \dot{s} = \ddot{s} = \ldots = s^{(n-1)} = 0 \tag{3.15}$$

When we talk about the higher order sliding mode control, we mean in particular the second order sliding mode. The design of second order sliding mode control shows a variety of algorithms in the liturature. The most applicable algorithms proposed in literature are: twisting control, sub-optimal control, super twisting control[40; 41].

3.3.1. Super twisting Control

Super-twisting algorithm was proposed by Levant [40; 41]. Since an n^{th} order sliding mode control algorithms require information about $S, \dot{S}, \ddot{S}, ..., S^{(n-1)}$, this algorithm can provide a continuous control by using only the information on S and the evaluating of the sign of $\dot{S}$ is not necessary. The convergence of this algorithm is also described by the rotation around the origin of the phase diagram $(S, \dot{S})$.

The super twisting algorithm has the advantage over the other algorithms that it does not demand the time derivatives of sliding variable. The super twisting (ST) control law *u(t)* is formed by two parts. The first discontinuous term is defined by its derivative with respect to time u_1 while the second is given by the function of the sliding variable u_2. The ST control law is defined by:

$$u_{ST} = u_1(t) + u_2(t) \tag{3.16}$$

$$\begin{cases} u_{ST} = -\lambda |s|^{\frac{1}{2}} sign(s) + u_1 \\ \dot{u}_1 = -\beta_\omega sign(s) \end{cases} \tag{3.17}$$

λ and β are positive gains used to adjust the ST controller.

The control law convergence can be reached by an arbitrarily adjusting of these gains [42]. Generally, the gain λ is more effective in system response. The gain β has an effect in steady state accuracy. The sufficient conditions for a finite-time convergence are imposed by Levant [41] as:

$$\begin{cases} \beta > \dfrac{\Phi}{\Gamma_M} \\ \lambda \geq \dfrac{4\Phi\Gamma_M(\beta+\Phi)}{\Gamma_m^3(\beta-\Phi)} \end{cases} \tag{3.18}$$

Φ is defined as the positive bounds of the uncertain function ϕ. Γ_m and Γ_M are the lower and the upper positive bounds of the uncertain function γ at the second derivative of the sliding manifold [41; 42],

The degree of nonlinearity can be adjusted by the coefficient ρ which is defined in the interval ($0 < \rho \leq 0.5$). It is fixed mostly at "0.5" to realize that the maximum of second order sliding mode control is achieved [42]. The controlled system can be simplified when it is linearly dependent on the control law *u*.

3.4. Improved direct torque control using sliding mode control

In this section, first and second order sliding mode controller will be designed for speed regulation loop to generate the electromagnetic toque reference and to ensure good dynamic and fast response.

3.4.1. First order SM-speed controller design

The sliding surface of the rotor speed is defined by:

$$\begin{cases} S_{\omega_r} = \omega_r^* - \omega_r \\ \dot{S}_{\omega_r} = \dot{\omega}_r^* - \dot{\omega}_r \end{cases} \tag{3.19}$$

The mechanical equation of PMSM is given as:

$$\dot{\omega}_r = \frac{1}{J}(T_e - T_L) - \frac{f}{J}\omega_r \tag{3.20}$$

By substituting the equation (3.66) in the equation of the speed surface derivative, it will be given as follow:

$$\dot{S}_\omega = -\frac{1}{J}(T_t - T_L - f\,\omega_r) \tag{3.21}$$

Basing on sliding mode theory, we can write:

$$T_e = T_{eeq} + T_{en} \tag{3.22}$$

The equivalent control part is defined during the sliding mode state $\dot{s}_\omega = 0$, then the equivalent control is:

$$T_{eeq} = f\,\omega_r + T_L \tag{3.23}$$

The discontinuous part is defined as:

$$T_{en} = K_{\omega_r} sign(S_{\omega_r}) \tag{3.24}$$

K_{ω_r} is a positive gain.

3.4.2. Second order SM-speed controller design

The second order sliding mode speed control law will be designed by the combination of the equivalent control and the super twisting control law. The super twisting speed controller (STSC) design is given as:

$$\begin{cases} u_{ST} = -\lambda_{\omega_r} \left| S_{\omega_r} \right|^{\frac{1}{2}} sign(S_{\omega_r}) + u_1 \\ \dot{u}_1 = -\beta_{\omega_r} sign(S_{\omega_r}) \end{cases} \tag{3.25}$$

λ_{ω_r} and β_{ω_r} are the super twisting speed controller gains.

The diagram of DTC-SVM control scheme with sliding mode controller is presented in **Fig.2.12**

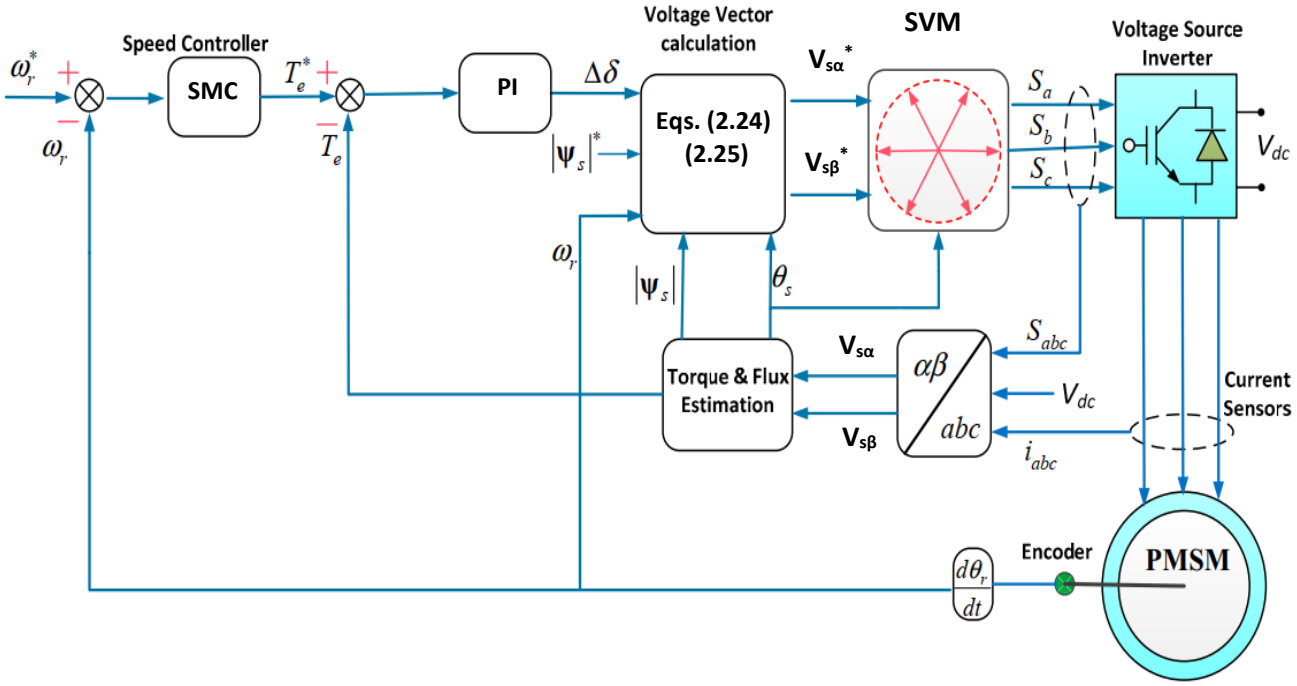

Fig.3.5: Block diagram of SVM-Direct torque control of PMSM.

3.5. Conclusion

This chapter presents a performance enhancement on SVM-direct torque control. First and second order sliding mode controllers have been used instead of the PI controller in the speed loop.

The next chapter will present the simulation results using MATLAB/Simulink as comparative study between the different control techniques

4.1. Introduction

This chapter presents the simulation of direct torque control algorithms presented in the previous chapter. All simulations have been implemented in Simulink, the software provides an interactive graphical environment and a customizable set of block libraries that let you design, simulate, implement and test a variety of time-varying systems. This makes it simpler to visualize and rapidly develop a control system unlike traditional C or MATLAB-code.

A comparative study between the switching table classical DTC and the direct torque control with SVM (SVM-DTC) is presented. The simulation has been conducted for three phases *3 kW PMSM* with characteristics given in the **Appendix A.1**

The operation conditions have employed for both control methods are: the starting up and the steady states followed by load introduction. The second simulation section presented DTC-SVM with different speed controllers

4.2. Simulation Results

4.2.1. Conventional DTC and SVM bases DTC comparative study

Figs.4.1-4.2 present the Simulink blocs of conventional direct torque control and improved direct torque control using SVM respectively

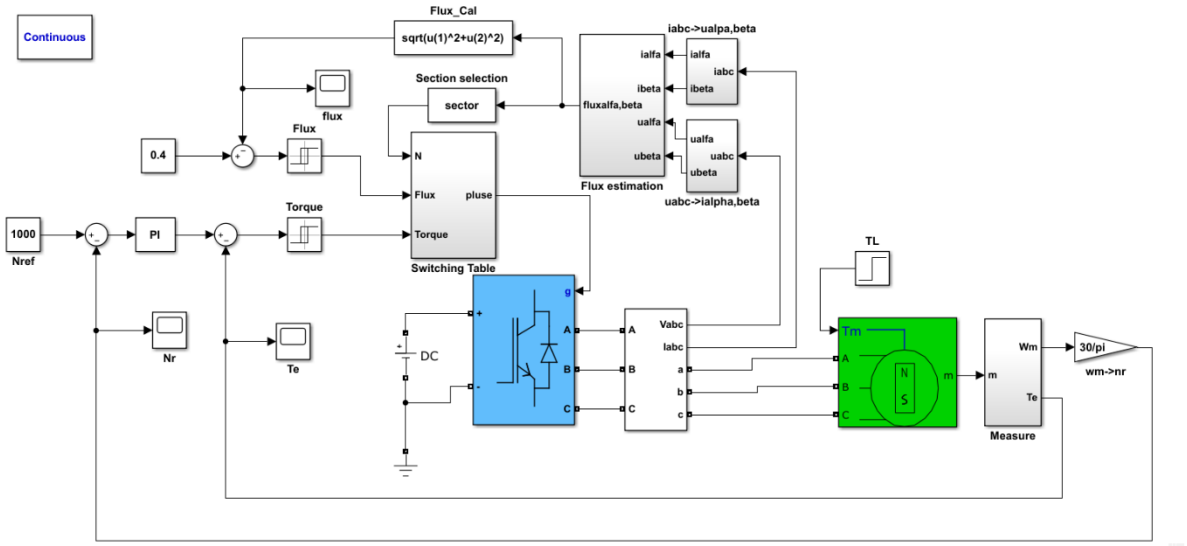

Fig.4.1: Conventional DTC Simulink Model

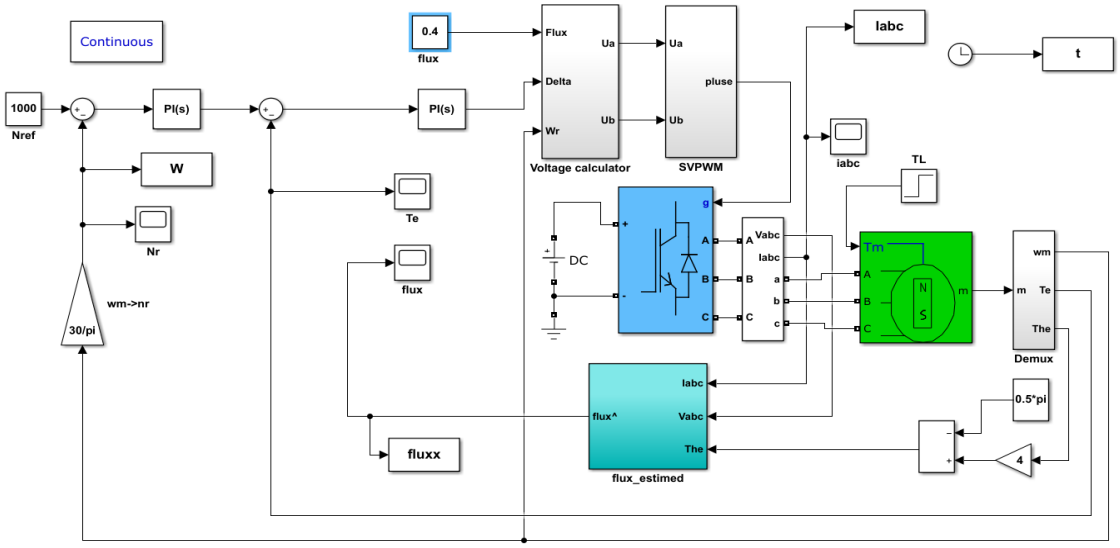

Fig.4.2: DTC-SVM Simulink model.

The following figures displays different simulation of conventional and improved direct torque control as a comparative study.

(a), For Conventional DTC **(b)** For DTC-SVM

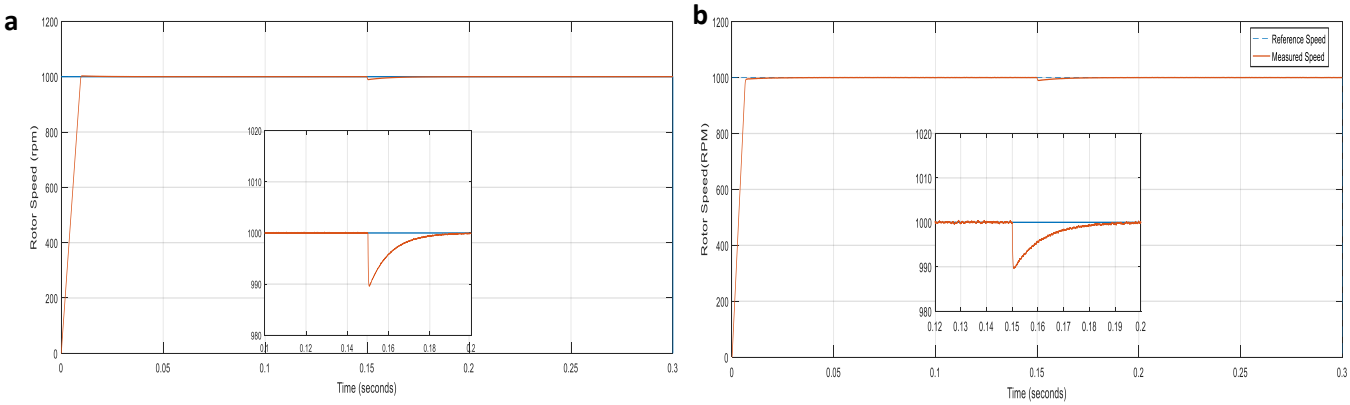

Fig.4.3: Rotor speed response at the starting up and steady states followed by load application.

The displayed simulation results above (**Figs.4.3**) show the starting up and the steady states with load application for the DTC controlled PMSM. **Fig.4.3** illustrates the comparison between speed responses of conventional DTC and SVM-DTC according to the speed reference step of 1000 rpm. The load disturbance has been introduced at (t=0.5s). The figure shows that both techniques show good dynamic at starting up. We can notice that the speed regulation loop rejects the applied load disturbance quickly. The SVM-DTC in **Fig.4.3(b)** kept the same fast speed response of DTC strategy. Since the same PI speed controller is used for both schemes, there is no difference in the transient response.

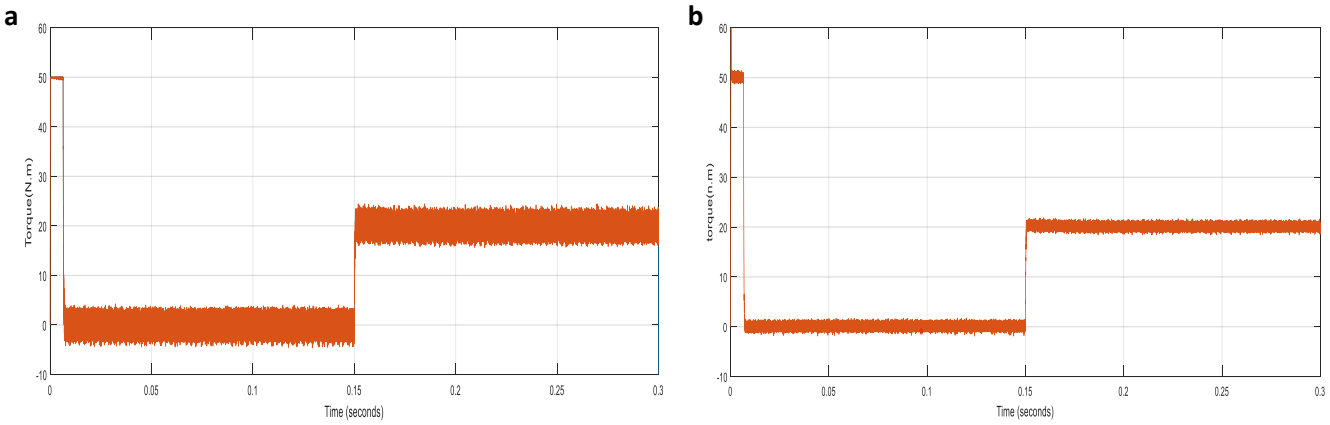

Fig.4.4: Electromagnetic torque with load application

Then, **Fig.4.4** illustrates the torque responses with by load application. The figure shows that at the beginning the speed controller (PI anti-windup) operates the system at the physical limit. It can be seen clearly that the constant switching frequency-based DTC strategy in **Fig.4.4(b)** has a reducer ripples level owing to the use of SVM compared to the conventional DTC in **Fig.4.4(a)**, where it is observed that the high torque ripples exceed the hysteresis boundary.

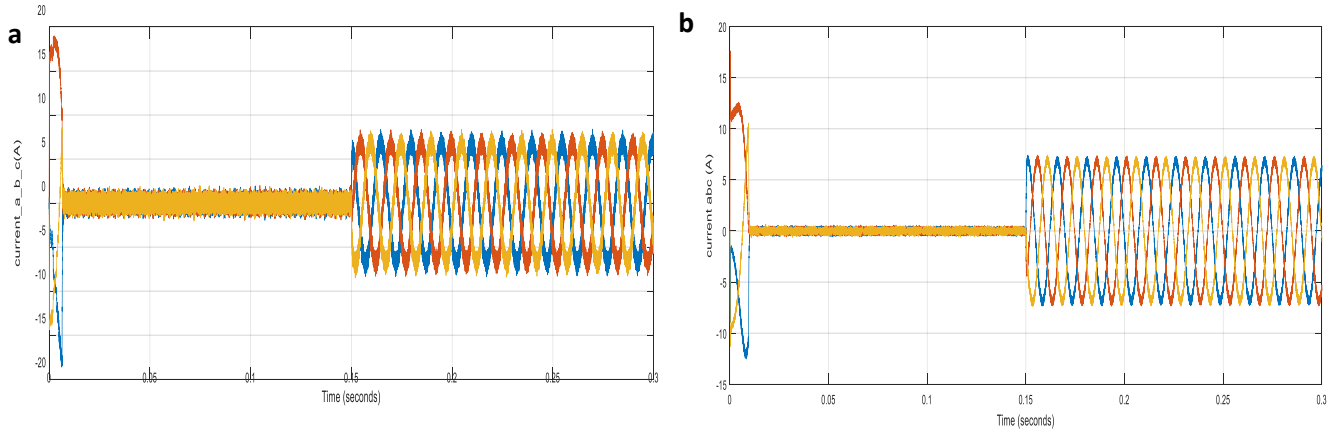

Fig.4.5: Stator phase currents i_{sabc}

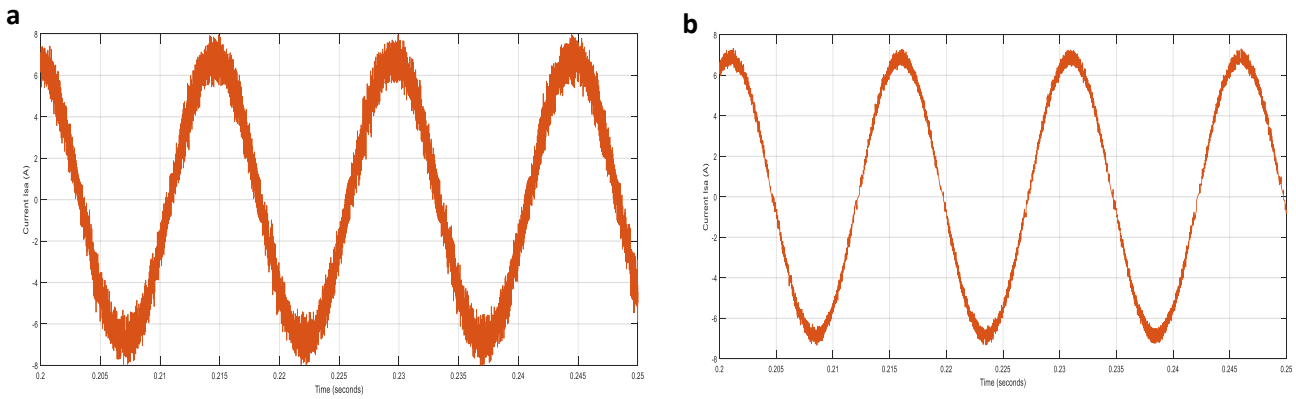

Fig.4.6: ZOOM of stator phase current i_{sa}

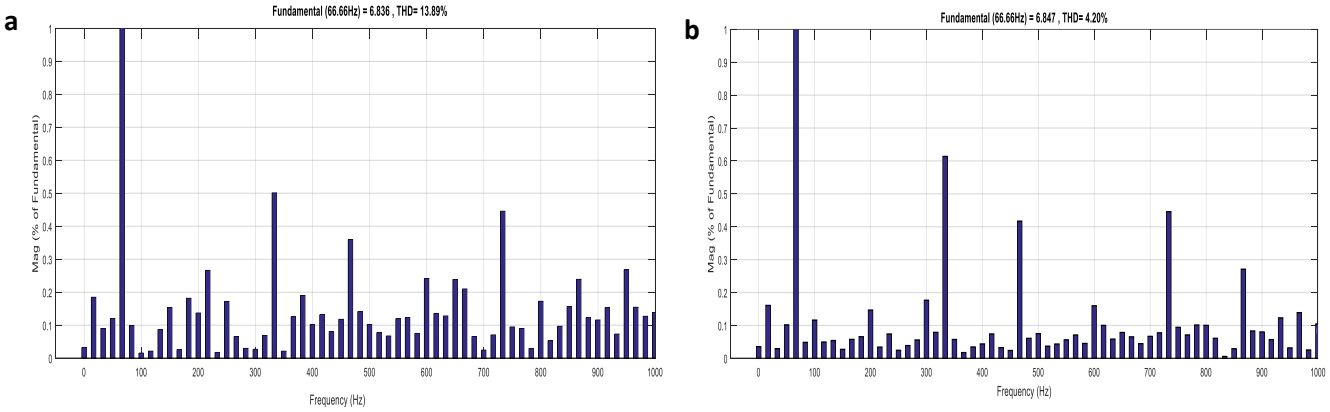

Fig.4.7: FFT analysis and spectrum of THD for stator phase current i_{sa}

Next, in **Figs.4.5-4.6**, the stator phase current with ZOOM and its FFT analysis are presented. It can be justified in the next figure where SVM-DTC has lower THD level (total harmonics distortion), 4.20% in **Fig.4.7(b)** compared to 13.89% for the classical DTC in **Fig.4.7(a)**.

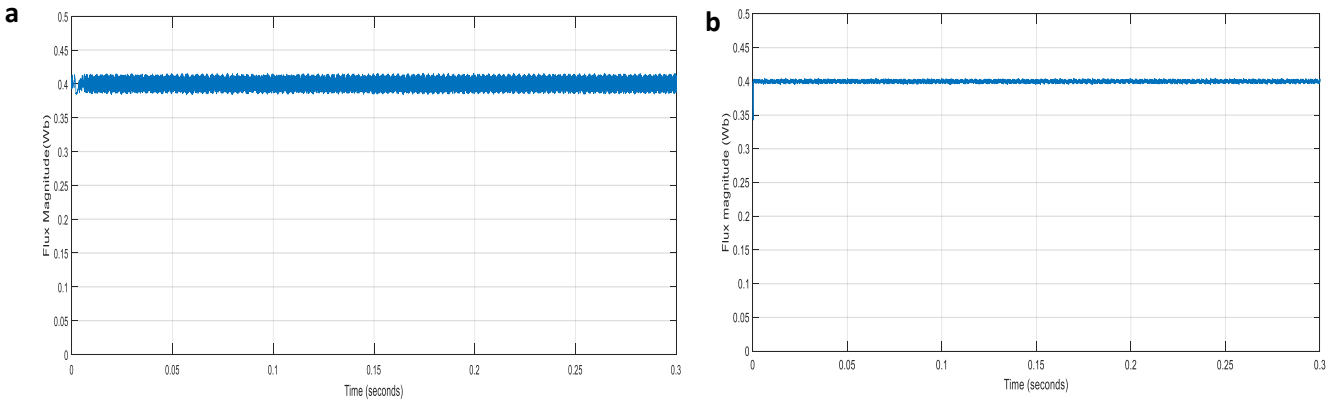

Fig.4.8: Stator flux magnitude [Wb].

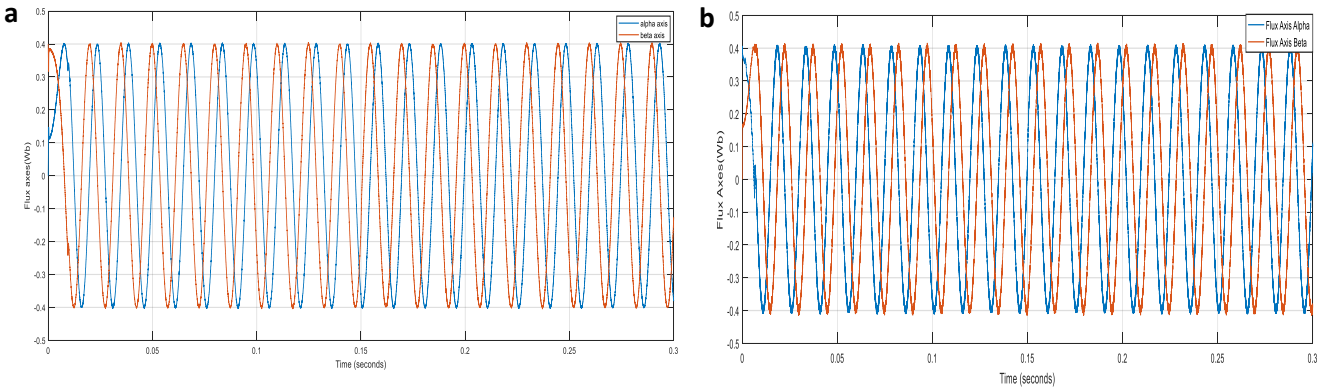

Fig.4.9: Stator flux components.

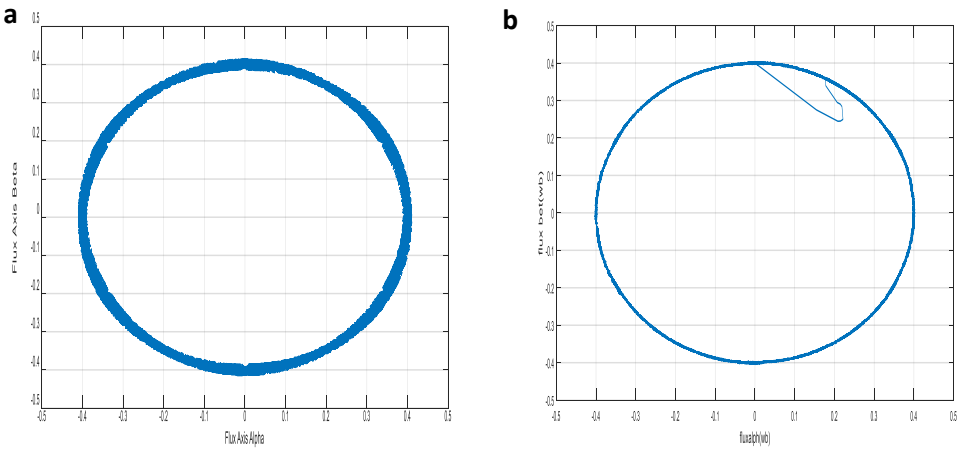

Fig.4.10: Flux circular trajectory (α,β) [Wb].

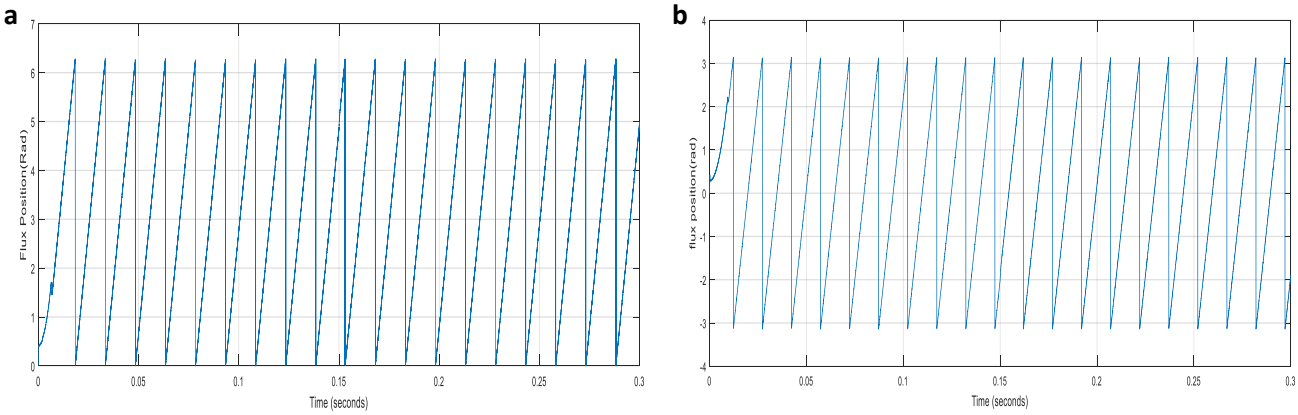

Fig.4.11: Position of stator flux vector.

After that, **Figs.4.8-4.10** exhibit the stator flux evolution (i.e. stator flux magnitude, components and circular trajectory). In **Fig.4.5(a)**, it is clear that the flux ripples of the conventional DTC have exceeded the hysteresis boundary. The magnitude and the trajectory illustrate that the flux takes a few steps before reaching the reference value (1Wb) at the starting stage due to the zone's changing (**Fig.4.10(a)**). The stator flux components show an acceptable waveform but high ripples level (**Fig.4.9(a)**). The SVMDTC in **Figs.4.10(b)** shows a reducer flux ripples, faster magnitude tracking at the starting up and better components waveform than the conventional DTC. **Fig.4.11** presents the position of the stator flux vector.

4.2.2. Speed regulation improvement using sliding mode control

This section presents the comparative study of different speed controllers, PI controller **(a)**, first order sliding mode controller **(b)** and second order sliding mode controller **(c)**

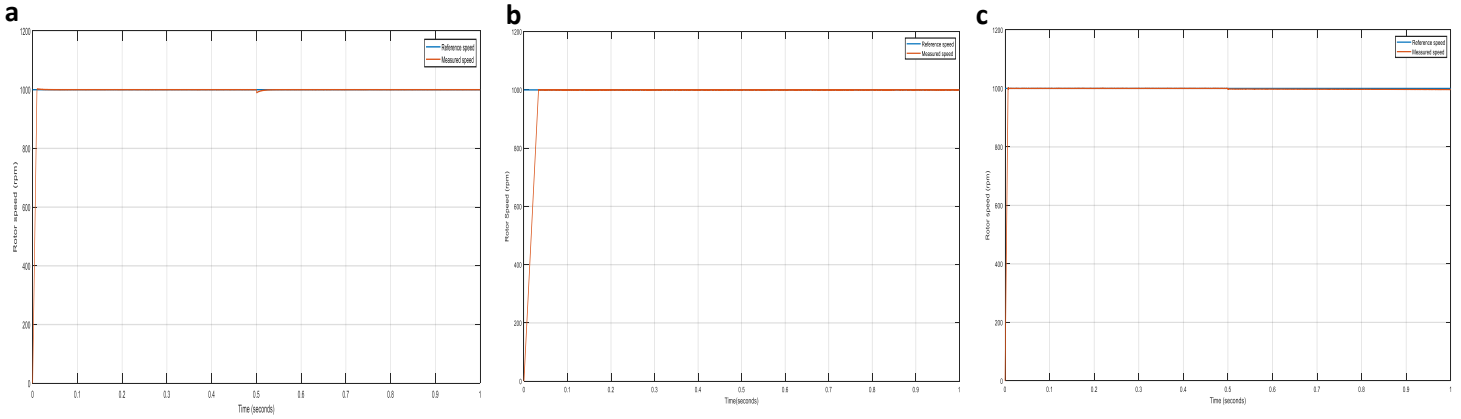

Fig.4.12 Rotor speed with load introduction (rpm).

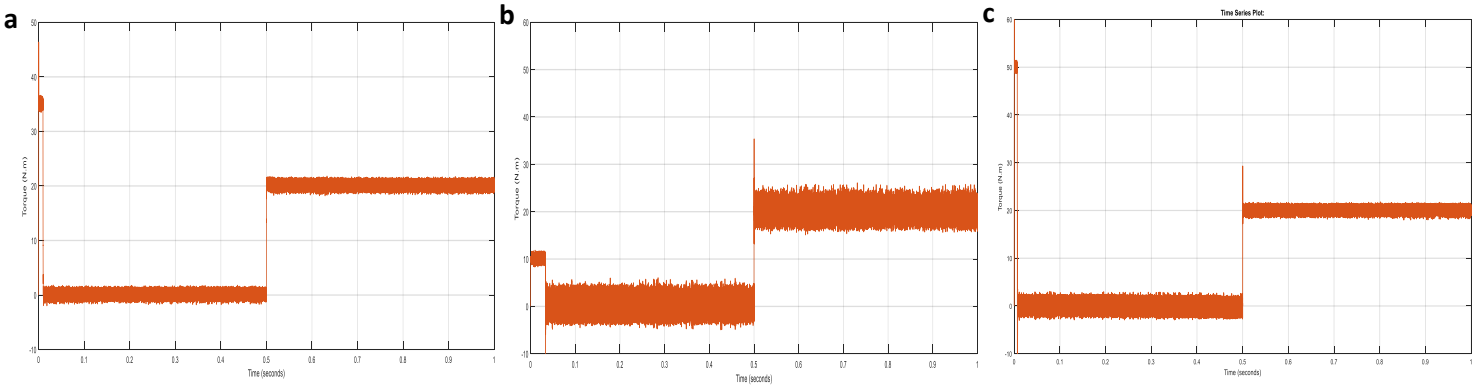

Fig.4.13: Electromagnetic torque (N.m).

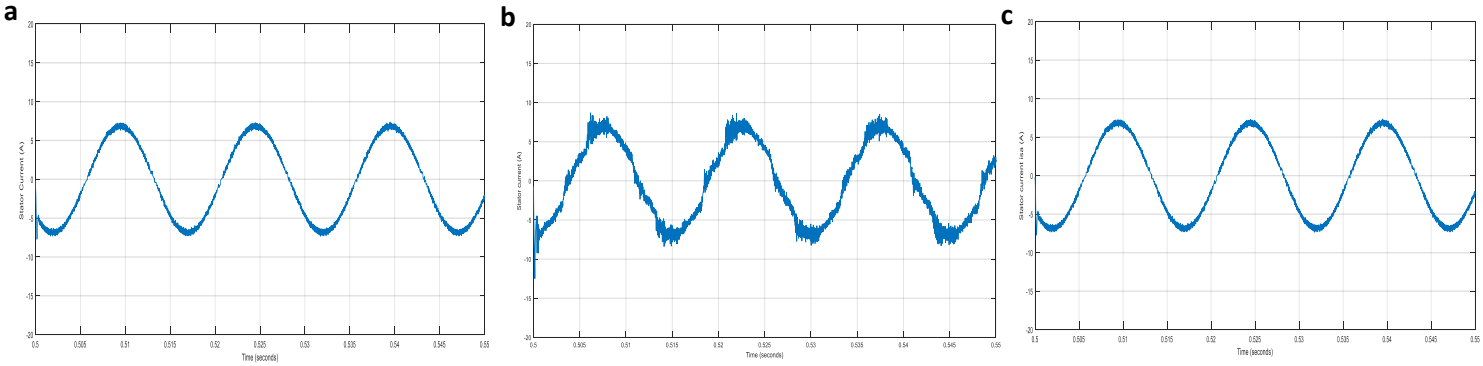

Fig.4.14: Stator phase current Isa (A)

Figs.4.12-4.14 illustrate the rotor speed, the electromagnetic torque and stator phase current to the control algorithm associated with PI, first order and second order sliding mode controllers during starting up and speed followed by load application of 20 N.m. The super twisting controller presents faster speed and torque responses compared with classical PI and First order sliding mode control. In addition, both first and second sliding mode controllers,

don’t affected by load introduction compared with PI. However, the first order sliding mode control show high torque ripples and chattering, this phenomenon has been avoided by second order super twisting controller. It can be proved in stator current in Fig.4.14, where the first order sliding mode controller show high distorted current while the PI and super twisting preserved a smooth sinusoid current waveform

4.3. Conclusion

This chapter present the simulation results of different control techniques presented in previous chapters. The simulation results have been presented into two sections, a comparative study between classical DTC and DTC with SVM. The comparisons of different controller based on sliding mode approach in the speed loop. The results show that the DTC-SVM can reduce considerably the flux, torque ripples and current harmonics and overcome DTC drawbacks. Furthermore, the sliding mode control can provide a robust control against load disturbances. Besides, the use of super twisting algorithm can solve the problem of chattering of sliding mode control.

General Conclusion

This dissertation deals with the enhancement of the direct torque control for Permanent Magnet Synchronous Motor. DTC is a control method which offers a decoupled torque and flux control for the electrical drives. As an alternative to the vector control, it is featured by simple structure, fast torque dynamic and less sensitivity to the machine parameters. However, it suffers from the high flux and torque ripples and the variable switching frequency. As a result, they lead to an acoustical noise and more control difficulty in low speed regions which degrades the performance of the control algorithm.

The main objective of this thesis is the improvement of the performance of a PMSM drive controlled by DTC using various control approaches. In this context, the research work has been addressed four principal points concerning the DTC control algorithm to be treated:

1. The reduction of high ripples and harmonics level which caused by the variable switching frequency due to the use of hysteresis comparators,
2. The designing of a nonlinear control law to improve the stability and robustness of control scheme while the presence of uncertainties.

Related to the control algorithms of the PMSM, the first chapter has presented an overview and modeling of PMSM. The second chapter has presented a brief theoretical about the classical DTC based on switching table and the constant switching frequency DTC based on the space vector modulation. The third chapter has presented the injection of sliding mode control law on SVM-DTC. The sliding mode control has been applied in the outer speed loop instead of the conventional PI controller to enhance compressively the control stability and robustness against external load disturbance. The second order sliding mode control was able to eliminate the phenomenon of chattering which made by the first order SMC and keep its same good performance like fast dynamic and simplicity. The comparative simulation results have presented in the 4^{th} chapter.

Future prospect

For the continuity of research, the future work could be oriented to a vaster area in this field, among our perspectives:

- Perform the experimental implementation for different presented control strategies to the PMSM.
- Development of sensorless control strategies for the PMSM drive.
- Development of the loss minimization and efficiency improvement strategy.

Appendices

A.1 Appendix 1

PMSM characteristics

Stator resistances Rs=2.3;

D-axis self-inductance Ld=0.0076;

Q-axis self-inductance Lq=0.0076;

Inertia moment J=0.0032;

Frication coefficient F=0.0004;

Number of poles pairs p=4;

Maximum flux ψ_s =0.4;

A.2 Appendix 2: Speed PI controller's gains calculation

The used PI controller in the outer speed loop for all control schemes is the anti-windup controller. The dynamic equation and the transfer function using Laplace transform of the speed loop are given as following:

$$\frac{d\omega_r}{dt} = -\frac{f}{J}\omega_r + \frac{T_e}{J} - \frac{1}{J}T_L \tag{A.1}$$

$$G_{\omega_r}(s) = \frac{\omega_r(s)}{T_e(s) - T_L(s)} = \frac{1}{Js + f} \tag{A.2}$$

The transfer function (TF) of the PI controller is defined as follow:

$$PI = K_p s + \frac{K_i}{s} \tag{A.3}$$

K_p and K_i are the proportional and integral gains.

s is Laplace operator

Then, **Fig.A.1**. shows the block diagram of the speed control loop.

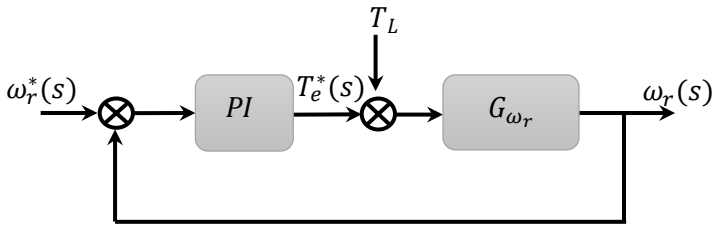

Fig.A.1 Speed control loop.

By considering the load torque T_L as a disturbance. The global transfer function of the speed control in open loop becomes:

Appendices

$$G_{\omega_r}(s) = \frac{\omega_r(s)}{\omega_r^*(s)} = \frac{1}{Js+f}\left(K_p s + \frac{K_i}{s}\right) \tag{A.2}$$

In closed loop, the TF becomes

$$G_{\omega_r}(s) = \frac{K_p s + K_i}{Js^2 + \left(K_p + f\right)s + K_i} \tag{A.3}$$

By identification member to member, the denominator of the equations (A.31) with the canonical form of second order system given in (A.32):

$$G(s) = \frac{1}{s^2 + 2\xi\omega_n s + \omega_n^2} \tag{A.4}$$

where ω_n is the natural frequency and ξ is the damping coefficient.

we obtain:

$$\begin{cases} \dfrac{J}{K_i} = \dfrac{1}{\omega_n^2} \\ \dfrac{K_p + f}{J} = 2\xi\omega_n \end{cases} \tag{A.5}$$

The gains are determined for a damping coefficient $\xi = 1$.

[1] Bose B (2002) Modern power electronics and ac drives. Prentice Hall PTR, Upper Saddle River.

[2] Dariusz Świerczyński, M. Sc. Direct Torque Control with Space Vector Modulation (DTC-SVM) of Inverter-Fed Permanent Magnet Synchronous Motor Drive.2005

[3] Chiasson J (2005) Modeling and high-performance control of electrical machines. Wiley, New York.

[4] Casadei, F. Profumo, G. Serra, and A. Tani, "FOC and DTC: Two viable schemes for induction motors torque control," IEEE Trans. Power Electron., vol. 17, no. 5, pp. 779–787, 2002.

[5] K. Hasse, "Drehzahlgelverfahren für schnelle umkehrantriebe mit stromrichte-rgespeisten asynchron-kurzschlusslaufer-motoren," *Reglungstechnik*, vol. 20, pp. 60–66, 1972.

[6] F. Blaschke, "The principle of field orientation as applied to the new transvector closed-loop control system for rotating machines," *Siemens Review*, vol. 39, no. 5, pp. 217–220, 1972.

[7] Takahashi, T.Noguchi, "A new quick-response and high-efficiency control strategy of an induction motor," IEEE Trans. on Ind. Appl., Vol.22, No.5, pp.820-827, 1986.

[8] M. Depenbrock, "Direct Self Control (DSC) of Inverter Fed Induction Machine", IEEE Trans. on Power Electronics, Vol. 3, No.4, pp.420-429, 1988.

[9] Isao Takahashi and Toshihiko Noguchi. A new quick-response and highe Efficiency control strategy of an induction motor. IEEE Transaction on industry applications, IA-22(5):820{827, 1986. Original article in japanese.

[10] M. Depenbrock. Direct self-control (dsc) of inverter-fed induction machine.IEEE Transaction on power electronics, 3(4):420{429, 1988. Original article in german.

[11] N. R. N. Idris and A. H. M. Yatim, "Direct torque control of induction machines with constant switching frequency and reduced torque ripple," IEEE Trans. Ind. Electronics, vol. 51, pp. 758-767, 2004.

[12] Riad TOUFOUTI "Contribution à la commande directe du couple de la machine asynchrone » Ph.D. thesis, University of Constantine, Algeria, 2008.

[13] Sebti Belkacem " Contribution à la commande directe du couple de la machine asynchrone » Ph.D. thesis, Bejaia University, Algeria, 2016..

[14] B. Bossou_, M. Karim, A. Lagrioui, and S. Ionit__a. Performance analysis of direct torque control (dtc) for synchronous machine permanent magnet(pmsm). 2010 IEEE 16th International Symposium for Design and Technology in Electronic Packaging (SIITME), pages 237{242, 2010..

[15] Dariusz Świerczyński "Direct Torque Control with Space Vector Modulation (DTC-SVM) of Inverter-Fed Permanent Magnet Synchronous Motor Drive" Ph.D. thesis, Warsaw University of Technology, Warsaw, Poland, 2005.

[16] Samira BENAICHA "Contribution à la commande toleranteaux defauts d'un systeme a motorisation asynchrone "apport de l'intelligence artificielle pour l'aide à la supervision et à la décision" Ph.D. thesis, University of Batna, Algeria,2010.

[17] Salih Baris Ozturk "direct torque control of permanent magnet synchronous motors with non-sinusoidal back-emf" Ph.D. thesis, Texas A&M University, 2008

[18] Antoni Arias Pujol "Improvements in direct torque control of induction motors" Ph.D. thesis, Universitat politécnica de Catalunya, Terrassa, 2000.

[19] Z. Zhang, C. Wei, W. Qiao and L. Qu, "Adaptive Saturation Controller-Based Direct Torque Control for Permanent-Magnet Synchronous Machines", IEEE Transactions on Power Electronics, pp. 7112-7122, 2016.

[20] Marcin Żelechowski "Space Vector Modulated – Direct Torque Controlled (DTC – SVM) Inverter – Fed Induction Motor Drive" Ph.D. thesis, Warsaw University of Technology, Warsaw, Poland, 2005.

[21] T. G. Habetler, F. Profumo, M. Pastorelli, and L. M. Tolbert, "Direct torque control of induction machines using space vector modulation," Ind. Appl. IEEE Trans., vol. 28, no. 5, pp. 1045–1053, 1992

[22] A. Ammar, A. Bourek and A. Benakcha, "Modified load angle Direct Torque Control for sensorless induction motor using sliding mode flux observer", in 2015 IEEE 4th International Conference on Electrical Engineering (ICEE) Proceeding, Boumerdes, Algeria, 2015.

[23] Freddy Garces, Victor M. Becerra, Chandrasekhar Kambhampati and Kevin Warwick "Strategies for Feedback Linearization, A Dynamic Neural Network Approach" Springer-Verlag London Ltd 2003.

[24] T. Orlowska-Kowalska "Advanced and Intelligent Control in Power Electronics and Drives" Springer International Publishing Switzerland 2014.

[25] V. Panchade, R. Chile and B. Patre, "A survey on sliding mode control strategies for induction motors", Annual Reviews in Control, vol. 37, no. 2, pp. 289-307, 2013.

[26] S.V. Emelyanov, Variable Structure Control Systems (Nauka, Moskwa, 1967).

[27] V.I. Utkin, Variable structure systems with sliding modes: a survey. IEEE Trans. Autom. Control 22(2), 212–222,1977.

[28] V.I. Utkin, "Sliding mode control design principles and applications to electric drives", IEEE Transactions on Industrial Electronics, vol. 40, no. 1, pp. 23-36, 1993.

[29] T. Orlowska-Kowalska, G. Tarchala, M. Dybkowski “Slidingmode direct torque control and sliding-mode observer with a magnetizing reactance estimator for the field-weakening of the induction motor drive”, Math. Comput. Simul. Vol 98, April 2014, pp 31-45.

[30] S. M. Gadoue, D. Giaouris, and J. W. Finch, "Sensorless Control of Induction Motor Drives at Very Low and Zero Speeds Using Neural Network Flux Observers," IEEE Transactions on Industrial Electronics, vol. 56, pp. 3029-3039, 2009.

[31] Huangfu Yi-geng “Research of Nonlinear System High Order Sliding Mode Control and its Applications for PMSM” Ph.D. thesis, University of Technology of Belfort-Montbéliard And Northwestern Polytechnical University, France 2010.

[32] J.J. Slotine, C. Canudas de Wit, Sliding observers for robot manipulators. Automatica 27(5), 859–864 (1991).

[33] Muhammad Rafiq “Higher order sliding mode control based SR motor control system design” Ph.D. thesis, Faculty of Engineering, Mohammad Ali Jinnah University

Islamabad, June, 2012.

[34] Vadim Utkin, Jürgen Guldner, Jingxin Shi “Sliding Mode Control in Electro-Mechanical Systems” second edition, Taylor & Francis Group, LLC, 2009

[35] Heide Brandtstädter “Sliding Mode Control of Electromechanical Systems” Ph.D. thesis, Technische Universität München, Germany, 2009.

[36] BENDAAS Ismail “Contribution à la Commande Hybride par Mode Glissant Floue Appliquée à un Moteur à Induction. Apport des Techniques de L’intelligence Artificielle” Ph.D. thesis, University of Batna, Algeria,2016.

[37] A. Faqir, F. Betin, L. Chrifi Alaoui, B. Nahid and D. Pinchon, "Varying sliding surface control of an induction machine drive", in IEEE Conference on Control Applications Proceedings, 2003

[38] A. Benchaib, A. Rachid and E. Audrezet, "Sliding mode input-output linearization and field orientation for real-time control of induction motors", IEEE Transactions on Power Electronics, vol. 14, no. 1, pp. 3-13, 1999.

[39] H. Lee and J. Lee, "Design of Iterative Sliding Mode Observer for Sensorless PMSM Control", IEEE Transactions on Control Systems Technology, vol. 21, no. 4, pp. 1394-1399, 2013.

[40] A. Levant, “Sliding order and sliding accuracy in sliding mode control”, Int. Journal of Control, vol. 58, no. 6, June 1993, pp. 1247-1263.

[41] A. Levant, "Higher-order sliding modes, differentiation and output-feedback control", International Journal of Control, vol. 76, no. 9-10, pp. 924-941, 2003.

[42] M. Rashed, K. Goh, M. Dunnigan, P. MacConnell, A. Stronach and B. Williams, "Sensorless second-order sliding-mode speed control of a voltage-fed induction-motor drive using nonlinear state feedback", IEE Proceedings - Electric Power Applications, vol. 152, no. 5, p. 1127, 2005.

[43] Fengxiang Wang, “Model Predictive Torque Control for Electrical Drive Systems with and without an Encoder” Ph.D. thesis, Lehrstuhl fur elektrische Antriebssysteme und Leistungselektronik der Technischen Universitat München, 2014.

[44] T. G. Habetler, F. Profumo, M. Pastorelli, and L. M. Tolbert, “Direct torque control of induction machines using space vector modulation,” Ind. Appl. IEEE Trans., vol. 28, no. 5, pp. 1045–1053, 1992.

[45] C. Lascu, I. Boldea and F. Blaabjerg, "A modified direct torque control for induction motor sensorless drive", IEEE Transactions on Industry Applications, vol. 36, no. 1, pp. 122-130, 2000.

[46] J. Rodríguez, J. Pontt, César Silva, S. Kouro and H. Miranda “A Novel Direct Torque Control Scheme for Induction Machines with Space Vector Modulation” 35th Annual IEEE Power Electronics Specialists Conference Aachen, Germany, 2004.

[47] Isidori, A,, and A. Ruberti. “On the Synthesis of Linear Input-Output Responses for Nonlinear Systems,” *Sys.* & Contr. Lett., 4, 17,1984.